NOVA SCHOOL OF SCIENCE & TECHNOLOGY

DEPARTMENT OF PHYSICS

MARIA DOS SANTOS MARTINS

Bachelors Degree in Biomedical Sciences

BIOLOGICAL PROPERTIES AND MECHANISMS OF ACTION OF CAMPHOR-BASED METAL COMPLEXES FOR THERAPEUTIC PURPOSES

MASTER IN BIOMEDICAL ENGINEERING

NOVA University Lisbon
March, 2022

NOVA SCHOOL OF SCIENCE & TECHNOLOGY

DEPARTMENT OF PHYSICS

BIOLOGICAL PROPERTIES AND MECHANISMS OF ACTION OF CAMPHOR-BASED METAL COMPLEXES FOR THERAPEUTIC PURPOSES

MARIA DOS SANTOS MARTINS

Bachelors Degree in Biomedical Sciences

Adviser: Fernanda Marujo Marques
Main Investigator, Instituto Superior Técnico

Co-adviser: João Duarte Neves Cruz
Associate Professor, NOVA University Lisbon

MASTER IN BIOMEDICAL ENGINEERING

NOVA University Lisbon
March, 2022

Biological properties and mechanisms of action of camphor-based metal complexes for therapeutic purposes

To the ones that support me unconditionally.

Acknowledgements

Firstly, I would like to thank my advisor, Dr. Fernanda Marques, for guiding me through all the steps needed to reach the final goal of writing this dissertation. Thank you for all your patience, time and commitment.

I also need to thank Prof. Teresa Pinheiro who was, unofficially, my second advisor and shared with me an incredible amount of knowledge.

To my co-advisor, Prof. João Cruz, who inspired me during classes to choose this theme, for making me want to understand more about the applications of nuclear physics. Thank you for your availability and encouragement.

Additionally, I want to acknowledge all the people involved in this project: Joana Guerreiro for helping me perform the DNA-interaction studies, Rafaela Silva for the support provided in the stability studies, Prof. Fernanda Carvalho and Joana Costa for synthesizing the studied complexes and helping me understand every step of this process. Thank you all for your sympathy, for receiving me with open arms and always being available for answering my questions.

Finally, I want to thank my family, my friends and the friends who have become family.

To my parents, thank you for always believing that I am able of doing amazing things even when I don't. To my sister, who is the greatest part of me, my home, my comfort and my whole inspiration. To the rest of my family, for all the great times that made me forget all my problems and especially, to my grandparents who always inspired me to do and be better - thank you *Avó Ana* for making the world seem so easy and thank you *Avó Gina* and *Avô Avelino* for always looking out for me, I hope you're proud.

Thank you, my *"Ohana de Biomédica"*, for some of the best moments of my life, for never letting me give up. Without you, I know I wouldn't have done not even half of what I was able to do in these hard but wonderful six years. I want to specially acknowledge Mara Monteiro, who is my partner since day one and helped me overcome some of my hardest moments. Thank you for being my partner in crime, my "ride or die". And also, Diogo Silva, thank you for helping me calm down during times of crisis, for giving me comfort and making me laugh so hard when I needed the most.

Thank you to the rest of my colleagues and my academic family (Catarina Domingos, Daniela Martins, Francisca Alves and Raquel Gonçalves) for being such an important part of this journey. It wouldn't have been so fun without you.

Thank you to all my hometown friends. For being my safe net, for always being there when everything was falling apart. And especially to Mafalda Gonçalves, Mariana Alves and Diogo Cruz. For listening, for caring, for understanding and always being there. Thank you.

"Nothing in life is to be feared; it is only to be understood. Now is the time to understand more, so that we may fear less."
(Marie Curie)

Abstract

Surgical excision combined with chemotherapy with Cisplatin and its analogues is the main treatment for ovarian cancer. Although it is effective as first-line regime, 75% of the patients can experience recurrence and secondary effects, becoming vulnerable to develop resistance to chemotherapy and death.

The unique biological properties of camphorimine complexes based on different metal sources such as CuCl, $CuCl_2$, $Ag(NO_3)$, Ag(OAc) and $KAu(CN)_2$ anticipate their potential use as alternative to Cisplatin based therapies. The biological activity of silver camphorimine complexes against Cisplatin sensitive A2780 and Cisplatin resistant A2780cisR ovarian cancer cells have been previously described and the results obtained revealed that those complexes displayed higher activity than Cisplatin in the ovarian cancer cells and low toxicity in non-tumoral HEK 293 (human embryonic kidney) cells.

Encouraged by such results, the biological effects of different metals on the properties of camphorimine complexes were investigated in order to evaluate their potential therapeutic value. The cytotoxic activity of these complexes, their cellular uptake, cellular distribution and mechanism of action in OVCAR3 ovarian cancer cells were assessed.

Due to their high sensitivity in the detection of metals, ion beam techniques alone or combined in nuclear microscopy, were used to quantitatively evaluate the cellular uptake of the metal of interest and obtain images with micrometric resolution of the elemental distributions in single cells. The results indicate that the low cellular uptake of copper by OVCAR3 cells can explain the lower cytotoxicity of these complexes in relation to silver and gold analogues. Results highlight the importance of characterizing the cellular uptake and distribution in cells to have clues to the cellular targets and the mechanisms of action.

Keywords: Ovarian cancer, camphor derivatives, camphorimine metal complexes, cellular uptake, anticancer activity

Resumo

No tratamento do cancro do ovário, o plano terapêutico normalmente usado em contexto clínico inclui cirurgia combinada com ciclos de quimioterapia com Cisplatina ou compostos análogos. Este tratamento é inicialmente eficaz, mas 75% dos pacientes experiencia reincidência e efeitos secundários que os tornam mais vulneráveis ao desenvolvimento de resistência ao efeito da Cisplatina e eventualmente, à morte.

As propriedades biológicas de complexos metálicos de Cu(I), Cu(II), Ag(I) e Au(I) com ligandos de canforiminas revelaram o potencial de alguns desses complexos para serem usados para fins terapêuticos em alternativa à Cisplatina. De facto, em estudos anteriores, a atividade biológica de complexos de prata com ligandos de canforiminas demonstrou ser promissora. Estes compostos revelaram maior atividade citotóxica do que a Cisplatina em relação a células cancerígenas do ovário e baixa toxicidade para células não tumorais HEK 293. Estes resultados encorajaram os estudos desta dissertação. Os efeitos biológicos dos diferentes complexos metálicos com ligandos de canforiminas, foram estudados para avaliar o seu potencial terapêutico, nomeadamente, a atividade citotóxica destes complexos, a captação e distribuição celular e ainda, o mecanismo de ação nas células OVCAR3 do cancro do ovário.

Por apresentarem elevada sensibilidade na detecção de metais, técnicas de feixe de iões, isoladamente ou combinadas em microscopia nuclear foram utilizadas para avaliar quantitativamente a absorção celular do metal de interesse e obter imagens com resolução micrométrica das distribuições elementares em células isoladas.

Os resultados indicam que a baixa captação (uptake) celular de cobre pelas células OVCAR3 pode explicar a menor citotoxicidade destes complexos em relação aos análogos de prata e ouro com os mesmos ligandos. Os resultados realçam a importância de caracterizar o uptake e a distribuição celular nas células para se obter indicações sobre os alvos celulares e os mecanismos de ação.

Palavras-chave: Cancro do ovário, derivados da cânfora, complexos metálicos de canforiminas, captação celular, atividade antitumoral

Contents

List of Figures

List of Tables

Acronyms and Abbreviations

AAS	Atomic Absorbtion Spectroscopy
ATCC	American Type Culture Collection
ccc	Covalently Closed Circular
CT-DNA	Calf Thymus Deoxyribonucleic Acid
CTN	*Campus Tecnológico e Nuclear*
DMEM	Dulbecco's Modified Eagle Medium
DMSO	Dimethyl Sulfoxide
DNA	Deoxyribonucleic Acid
EBS	Elastic Backscattering Spectrometry
EOC	Epithelial Ovarian Cancer
FBS	Fetal Bovine Serum
FDA	Food and Drug Administration
GI	Gastrointestinal
HDF	Human Dermal Fibroblasts
HEK	Human Embryonic Kidney
IBA	Ion Beam Analysis
ICP-MS	Inductively Coupled Plasma Mass Spectrometry
IST	*Instituto Superior Técnico*
MDA	Malondialdehyde
MTT	3-(4,5-dimethythiazol2-yl)-2,5-diphenyl tetrazolium bromide

NADH Nicotinamide Adenine Dinucleotide + Hydrogen
NBT Nitro Blue Tetrazolium
NHC N-heterocyclic carbenes

oc Open Circular

PBS Phosphate-Buffered Saline
PIXE Particle Induced X-ray Emission

ROS Reactive Oxygen Species
RPMI Roswell Park Memorial Institute

SD Standard Deviation
SI Selectivity Index
SOD Superoxide Dismutase
SR-XRF Synchrotron Radiation X-Ray Fluorescence
STIM Scanning Transmission Micoscopy

TAE Tris-acetate-EDTA
TBA Thiobarbituric Acid
TBARS Thiobarbituric Acid Reactive Substances
TrxR Thioredoxin Reductases

UV Ultraviolet
UV-Vis Ultraviolet-Visible

WHO World Health Organization

1

Introduction

1.1 Motivation

Ovarian cancer is the second most common gynecologic malignancy and the leading cause of death among women [1].

Chemotherapeutic plans involving platinum-based drugs (Cisplatin and its analogous) are often prescribed and reveal high efficiency in the treatment of multiple types of cancer, including ovarian cancer. Despite that, the use of this class of drugs also causes the occurrence of significant secondary effects and increasing resistance in the treated patients. The need to solve this problem prompted the development of new metal-based compounds as alternatives to Cisplatin displaying anticancer properties while enhancing selectivity to cancer cells, reducing general toxicity for healthy tissues and also the side effects.

Complexes with transition metals have been receiving special attention for their unique properties and considerable potential as anticancer drugs. Several studies have been done exploring the biological effects of these compounds; some of them even reached clinical trials but were never approved for clinical practice. Complexes of copper, zinc, silver and gold are some of the most studied metal complexes and prior investigations demonstrated important biological behavior of silver camphorimine complexes, that have been considered as potential agents to treat ovarian cancer [2].

The relentless search for alternative drugs for ovarian cancer treatment is essential for a future where a more successful healthcare is provided to patients that suffer from this malignancy.

1.2 Objectives

The main goal of this dissertation was the evaluation of the therapeutic potential (in vitro) of copper (I and II), silver (I) and gold (I) complexes with camphorimine ligands (figure 1.1), monocamphor and bicamphor derivatives, for ovarian cancer.

Studies were undertaken to evaluate the biological behavior and the mechanism of action of the compounds presented in table 1.1 towards normal and ovarian cancer cells.

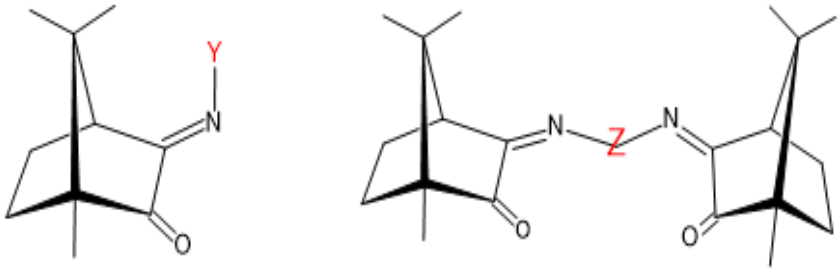

Figure 1.1: Camphorimine ligands: type A (monocamphor) (left), Y=C_6H_5(^{1}A); $C_6H_4NH_2$(^{2}A); type B (bicamphor) (right), Z= 4-C_6H_4(^{1}B), 3-C_6H_4(^{2}B).

Another key parameter to be evaluated when appraising therapeutic potential of metal complexes is the cellular uptake and distribution. For that purpose, the use of Ion Beam Analysis (IBA) techniques, in particular nuclear microscopy, with high spatial resolution and sensitivity has proven to be a powerful tool in providing information of metal trace concentrations inside the cells. Indeed, the use of IBA methods needs to be emphasized inasmuch as attributes an innovative character to this investigation - the combined use of IBA methods provided density and elemental distribution maps essential to visualize metal accumulation inside ovarian cancer cells.

The results provided by the techniques mentioned above helped to identify the mechanisms of action of the complexes listed in table 1.1.

Table 1.1: The camphorimine metal complexes studied in this work.

ID	Complex
1	$[(CuCl)_2(^2A)]$
2	$[CuCl_2(^1B)]\cdot 2H_2O$
3	$[(CuCl)_3(^2B)]$
4	$[CuCl_2(^1A)_2]$
5	$[Ag(NO_3)(^1A)_2]$
6	$[Ag(^1A)_2(\mu\text{-}O)]$
7	$[Ag(OH)(^2A)]CH_3COOH$
8	$K[Au(CN)_2(^1A)_3]\cdot 1/2H_2O$
9	$K[Au(CN)_2(^2A)]\cdot H_2O$

1.3 Structure of the Dissertation

This dissertation is composed by seven chapters and three appendixes.

In the present and first chapter, the motivation for the development of the studies and the established goals are described. On the second chapter, the fundamental theoretical concepts needed for the comprehension of the nuclear microscopy analytical techniques and associated physical phenomena are presented to the reader.

Following for chapter number three, one will find a meticulous description of the current state of the art on ovarian cancer, existing therapies, studies involving the assessment of the properties of metal-based complexes for cancer therapy and also, the application of precise imaging techniques for evaluating drug uptake in whole single cells.

All the methods and materials employed in the context of this dissertation and the results obtained from their application are fully described in chapters four and five, respectively. Both of these two chapters are divided in two major sections: Biological Assays and Cellular Uptake. The "Biological Assays"section is composed by all the information regarding cellular biology methods (cytotoxicity assay, stability studies, Deoxyribonucleic Acid (DNA)-interaction evaluation, Reactive Oxygen Species (ROS) and Malondialdehyde (MDA) production assessment). On the other hand, the "Cellular Uptake"unit is constituted by all the details associated to the nuclear microscopy setup, the imaging of the treated cells and the Macro-Particle Induced X-ray Emission (PIXE) process.

In chapter six, the results are extensively examined and the derived assumptions are explained. In the final chapter, the final conclusions are presented as well as the main obstacles and future perspectives for the developed theme.

2

Theoretical Concepts

2.1 Nuclear Microscopy Analytical Techniques for Quantitative Elemental Analysis in Cells

The evaluation of the dynamics of trace elements in biological systems is essential to understand vital processes in which these elements are involved. They participate as cofactors of enzymes and also have stabilization and structure functions. Some of the endogenous elements are essential in vestigial amounts and disequilibrium in their cellular concentrations can cause serious damage [3]. When the intention is to study the interaction of metallodrugs with cells, very simple cell cultures, probe tissues or model organisms are used. In an attempt to unravel the interaction of these metallo-complexes with cells, one of the relevant questions refers to the efficacy of cellular uptake. To achieve this goal, the metal of interest should be detected and quantified with high sensitivity. In addition, the visualization of the distribution of the elements of interest in a single cell with high-resolution and in conditions close to *in vivo* would help devising cellular targets of that specific drug.

Although, all the above mentioned requirements are difficult to unite in a single technique, ion probes based on the use of energetic particles enable to assemble a set of analytical techniques that can deliver images of single cells with relatively high resolution (micrometer range) and to perform quantitative analysis even in very small sample masses without significant loss of sensitivity. In such an ion probe we use accelerated ions such as protons, accelerated to energies between 1.5 and 2.5 MeV and focused to micrometre dimensions. The current and divergence of the beam are defined by slits at appropriate distance from the electrostatic lenses that focus the beam on the target plane. In most set-ups the target plane is located inside a vacuum chamber, where several detectors can be positioned in a defined geometry around the sample to detect physical phenomena induced by the interaction of energetic particles with atoms (figure 2.1). The focused beam is scanned over a sample region of interest, enabling to generate two-dimensional maps of the sample by extracting spectral information for each position of the beam.

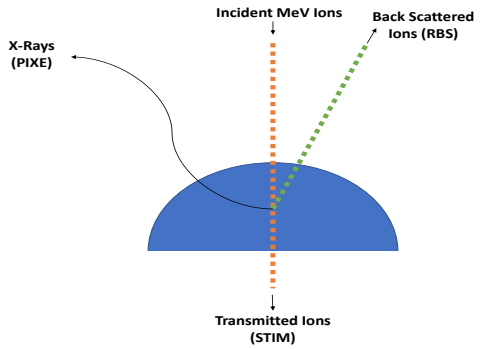

Figure 2.1: Products of the interaction of MeV ions with the biological sample and the associated imaging techniques used in the studies of the present dissertation. PIXE: particle induced X/gamma-ray emission. RBS: Rutherford backscattering spectrometry (also referred as elastic backscattered spectrometry). STIM: scanning transmission ion microscopy. Adapted from: [4]

There are three ion beam analytical techniques that can be used simultaneously giving spatial information, morphological and structural features and elemental quantification. The most useful techniques implemented in nuclear microscopy are, scanning transmission ion microscopy (Scanning Transmission Micoscopy (STIM)) in off-axis mode, Particle-Induced X-ray Emission (PIXE) and Elastic Backscattering Spectrometry (Elastic Backscattering Spectrometry (EBS)). The simultaneous use of these technique for the same sample offers cellular direct imaging of density and elemental distributions without using chemical and dyes, which may cause elemental leakage and/or their redistribution in cells [3, 5, 6].

2.1.1 Particle Induced X-ray Emission (PIXE)

The PIXE technique was initially developed by S. A. E. Johansson in 1970 [7]. PIXE is a fast sensitive multielemental analysis technique based on the induced emission of atomic characteristic X-rays. When a MeV ion interacts with an atom causes its ionization, creating a vacancy in an inner shell that will be occupied by an electron of an outer shell [3, 5]. For each transition, a photon is emitted (figure 2.2). The set of X-rays emitted by each atom (energies correspond to the difference between the binding energy of each subshell involved in the electronic transition) is characteristic of that atom, and therefore constitutes a signature of each element [8]. A spectra of multiple elements present in the sample can then be generated (figure 2.3) .

X-ray radiation is included in the electromagnetic spectrum with wavelengths between 10 and 0.01 nm (which cover an energy range of 0.12 keV to 120 keV). In atomic spectrometry, the electronic shells are usually denominated by transitions between the K, L and M atomic shells. For instance, when the vacancy is created in the K shell and filled by an electron from the L or M shells, the emitted X-rays are grouped in K_α and

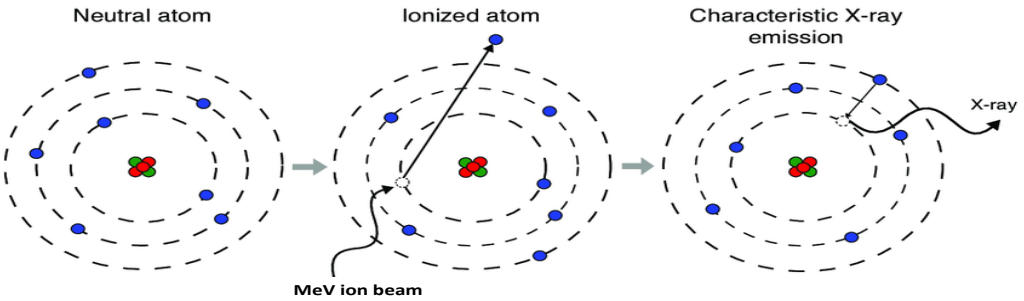

Figure 2.2: Process of induced emission of characteristic x-rays from an atom after interaction with an MeV accelerated ion beam. Obtained from: [9]

K_β lines, respectively. The same happens for the L and M emission lines. Due to energy degeneration and the energy sub-levels associated to each shell, additional notation was introduced - a number is used to specify which energy level is being considered (the K_α emission line includes $K_{\alpha 1}$ and $K_{\alpha 2}$, where the $K_{\alpha 1}$ emission is normally slightly higher in energy) [8].

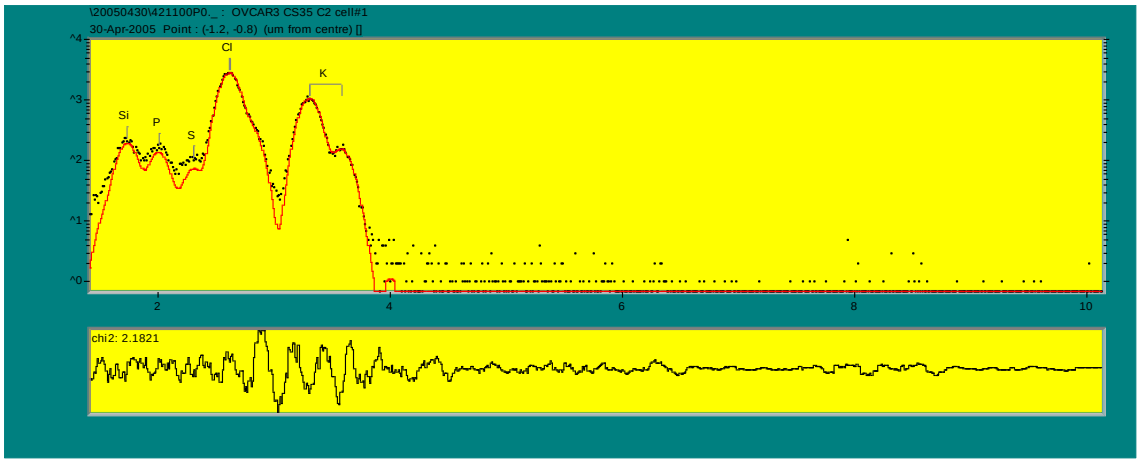

Figure 2.3: PIXE spectrum of an ovarian cancer cell (OVCAR3) using 2 MeV proton beam.

The PIXE technique is particularly appropriate for minor and trace elements detection in biological samples which correspond to atomic numbers, Z, ranging from sodium to lead ($11 \leq Z \leq 82$). PIXE shows a relatively high sensitivity for transition metals which are usually present as trace elements in biological samples. The detection limits depend on the element to be detected, the nature of the sample in analysis and the experimental and analytical conditions. However, the ability of this technique to detect trace elemental concentrations above $1\mu g/g$ of dry mass in tiny sample masses (I.e., corresponding to a volume under the microbeam of 1 to 10 μm^3) is what makes PIXE a very useful technique in nuclear microscopy [3, 5].

The PIXE technique enables full quantitative elemental analysis as a proportional relation can be established between the number of emitted X-rays and the number of

atoms in the sample. There is a linear relationship between elemental X-ray yields, i.e. the counts on the PIXE spectrum ($Y_p(Z)$) and the concentrations (C_z) given by a sensitivity factor ($K(E_z)$), for each atomic number (Z) with characteristic X-ray emitted energies (E_z), as expressed by equation 2.1.

$$Y_p(Z) = K(E_z)N_pC_z\Delta x \tag{2.1}$$

The elemental quantification by PIXE is based on an instrumental calibration, requiring knowledge of the experimental setup (e.g., position of the sample relative to incident beam, angle of X-ray detection, transmission parameters, among others). In this context the quantification method is absolute, requiring only beam charge adjustments (N_P) when analysing an unknown sample. In a microbeam setup and for tiny mass corresponding to the cell volume under the beam dimension, both the charge correction (N_p) and the matrix composition to estimate the sample thickness (Δx) are needed to normalize the X-ray yields of the PIXE spectra. This can be obtained for any mass core by analysing the EBS spectra [10]. The energy straggling, i.e., the spreading of energy distribution of the particles when they are slowed down by the interactions with the sample, can be neglected in this theoretical deduction without having significant impact on the results [8].

The advantages of PIXE stem on the microanalytical and multielemental capabilities without significant losses of sensitivity. For instance, Inductively Coupled Plasma Mass Spectrometry (ICP-MS) and Atomic Absorbtion Spectroscopy (AAS) are the gold standard in elemental analysis showing the best sensitivity (down to ppt level) although only bulk analysis are possible. In fact, PIXE presents very competitive sensitivity that makes it one of the most advantageous analytical tool to map trace elements in single cells and biological tissues [3, 5]. Additionally, PIXE is a fast process due to the high cross-section values associated to the process of ionization and emission of X-ray radiation. Other imaging modalities, such as scanning or transmission electron microscopy may be associated to X-ray detection at the microscale, although only concentrations in the % level are possible, which is not useful to single cell analysis. The recently developed X-ray fluorescence (Synchrotron Radiation X-Ray Fluorescence (SR-XRF)) nanoprobes making use of high-brilliance Synchrotron radiation offer excellent sensitivity for trace metal detection at lower spatial resolutions (below a few hundred nanometres), which surpass sub-micrometre spatial resolution obtained in nuclear microscopy PIXE routine setups. However, the elemental analysis is only qualitative [11, 12].

2.1.2 Elastic Backscattering Spectrometry (EBS)

One of the main problems with using PIXE as quantitative micro-analytical method is that the matrix composition and secondary electron emission might vary locally, originating uncertainties in the analysis. This is solved by the parallel use of EBS analysis that allows an internal standardization for obtaining absolute measurement - the EBS spectrum shape

is used to obtain the matrix composition while the total area bellow that same spectrum is indicative of the total beam charge. [6]

Elastic Backscattering Spectrometry (EBS) is based on measuring the energies of ions elastically scattered at angles greater than 90°. In a collision, a certain amount of energy is transferred to the recoiling particle, and the backscattered ion emerges with an energy, E1, that depends on the angle of scatter and the mass of the scattering nucleus, in agreement with the following relation:

$$K(\theta, M_1, M_2) = \frac{E_1}{E_0} = \left[\frac{(M_2^2 - M_1^2 \sin^2\theta)^{\frac{1}{2}} + M_2 \cos\theta}{M_1 + M_2} \right]^2 \tag{2.2}$$

where E0 is the incident energy, and M1 and M2 are, respectively, the mass of the ion and the mass of the scattering nucleus. The K factor, is known as the kinematic factor. From this equation, we conclude that in collisions with heavy nuclei the energy of the backscattered particle is higher. Plotting the number of counts versus energy, a spectrum is obtained and the composition of the sample is revealed by comparing with known scattering cross-sections [3, 5].

This method is sensitive to any element that is heavier than the incident ions but in biological samples, is specially well suited for bulk elements (like carbon, nitrogen, and oxygen that represent 90% of the cell mass) in detriment of trace elements. The concentration of trace elements is so reduced that, is not sufficient to produce significant and readable signal in the EBS spectrum. Besides depth distribution information, EBS also complements PIXE data, in terms of detection of light elements (PIXE doesn't assess the concentration of the already mentioned elements that EBS does), and EBS is used to measure the integrated charge of the incident beam during the irradiation process [3, 5].

2.1.3 Scanning Transmission Ion Microscopy (STIM)

The off-axis STIM relies on the detection and the analysis of the energy loss of forward scattered transmitted ions deflected off the beam axis by nuclear collisions at a small angle [13]. These energy loss values of the protons that did not suffer nuclear backscattering collisions depend on the density variations of the specimen. That is, STIM is a technique that measures the electron density variations in samples thin enough to transmit the beam, such as a cell. Based on the obtained data, images with resolution bellow 0.5 μm that reveal the cell boundaries and structure can be obtained [6].

The off-axis geometry associated to this process, considering scattering angles between 20° and 45°, results in a combination of the phenomenon of energy-loss dependent of the sample density with the mass dependent kinematic factor for the scattering caused by atoms like H, C and N [14]. The energy of the transmitted ions is measured, and the contrast is due to a combination of small-angle scattering and energy loss in the sample, which depend on the localized electron density in the sample. Therefore, a 2D areal density map can then be constructed. The technique is useful to depict structural

and morphological details of a cell that can be correlated with PIXE maps to associate elemental distributions with cellular compartments [6, 15].

3

State of the Art

3.1 Ovarian Cancer

According to World Health Organization (World Health Organization (WHO)), cancer may arise from the interaction of environmental agents (physical, chemical or biological) combined with the individual's genetic factors. This interaction disrupts normal mechanisms of the organism, resulting in uncontrollable growth of abnormal cells from old cells. This aggregation of cells is called a tumour that can grow anywhere in the body [16]. The classification of cancer can be done by the first location in the body (ovarian, lung, brain, etc.) where it started to develop and by its histological type, i.e. the kind of tissue where it originates. According to this last parameter, it is possible to distinguish between carcinoma, sarcoma, myeloma, leukaemia, lymphoma and mixed types (e.g. carcinosarcoma). Carcinomas, malignant neoplasms in the epithelial tissue, account for 80 to 90% of all cancer cases [17].

The ovarian cancer is a very heterogeneous condition as it comprises pelvic cancers with distinct tissues of origin, biology, development, symptoms, diagnosis and prognosis [18]. The official classification system defined by WHO divides ovarian neoplasms into epithelial, germ cell and sex cord-stromal neoplasms by their histological differences [17]. The epithelial ovarian cancer (Epithelial Ovarian Cancer (EOC)) is the ninth most common cancerous diagnosis presented in women worldwide and is associated to 95% of malignant tumors in the ovaries and to 46% survival 5 years after being diagnosed [1, 19, 20]. The acute presentation of EOC symptoms include, as stated by A. Desai et al. [1], "pleural effusion, small bowel obstruction and venous thromboembolism"and the subacute manifestation of this condition comes under the form of "nonspecific symptoms such as abdominal fullness, bloating, an adnexal mass, vague pelvic or abdominal pain and gastrointestinal symptoms". [20, 21].

The lack of specific symptoms, adequate screening methods that allow early detection and the disease's heterogeneity constitute the main obstacles to more effective health care services [19, 21]. Other factors may have impact on prognosis and need to be considered by the physician when prescribing a therapy plan. The individual's age and ??, the quality

and efficiency of the surgery and chemotherapy plan influence the survival rate [21].

3.2 Cancer Treatment

The most adequate therapeutic procedure depends on the type and stage of the cancer. The patient can be submitted to traditional therapies (e.g., surgery, chemotherapy, radiation therapy) or newer forms of treatment (e.g., immunotherapy, targeted therapy, hormone therapy, gene therapy, photodynamic therapy, proton therapy) [16].

Chemotherapy is one of the most used modalities to treat cancer. The main role is thus to kill the cancer cells while sparing the normal cells and tissues (at least with the most critical tissues, such as the bone marrow and the gastrointestinal tract). This has proven to be a challenge because cancer cells arise from normal tissue and most anticancer drugs have greater effect against high-growth-fraction tumours such as leukaemia and lymphoma, and the bone marrow and Gastrointestinal (GI) tract that have also a high cell-proliferation rate. Furthermore, the colon, rectum, lung, and breast tumours are the most common ones and present a low proportion of dividing cells, not being so susceptible to the drug effect alone [22]. Considering this and other limitations associated, some drugs are administered to the patient in combination with other drugs and/or other treatment modalities [16].

3.2.1 Ovarian Cancer Treatment

Normally, in cases of ovarian cancer, a surgical excision is performed followed by cycles of chemotherapy with Cisplatin (or its derivatives), in combination with other drugs to overcome the side effects and the developed resistance [16]. All the accessible malignant tissue is removed in the primary debulking surgical intervention and the remaining non-visible/not-reachable cancerous tissue is treated with the chemotherapeutic drugs.

The platinum (II) complex Cisplatin is the most used chemotherapeutic drug to treat various types of cancer, including ovarian cancer. Cisplatin is a diamminedichloroplatinum compound in which the two ammine ligands and the two chloro ligands are oriented in a cis planar configuration around the central platinum ion, as can be seen in figure 3.1 [16, 23, 24].

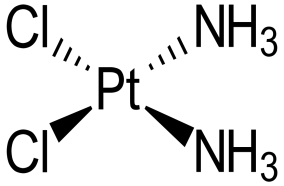

Figure 3.1: Cisplatin chemical structure. Obtained from: [25]

Cisplatin is administered to the patient by an intravenous via in a saline sterile solution that maintains Cisplatin stable in the bloodstream because of the existing high concentration of chloride. In contact with some proteins of the blood plasma (like albumin, transferin, etc.), Cisplatin bonds and 65% to 95% of the compound is inactivated 24 hours after being in circulation in the body. The remaining Cisplatin enters the cells by passive diffusion and through the copper transporters CTR1. These transporters suffer degradation with Cisplatin, decreasing cellular sensitivity to the drug [16].

There are multiple mechanisms of action associated to Cisplatin but the most common and well-described is the interaction with the DNA molecule [16]. Once cisplatin enters the cells, it immediately suffers the loss of one or both chlorine ligands due to the lower chloride concentration in the cells. This creates the opportunity to form a bond between the water present in the cellular milieu and the complex by a process called aquation. The aquated platinum product, the active species, reacts and crosslinks with DNA in the available sites (figure 3.2), resulting in the creation of DNA adducts. [16, 23].

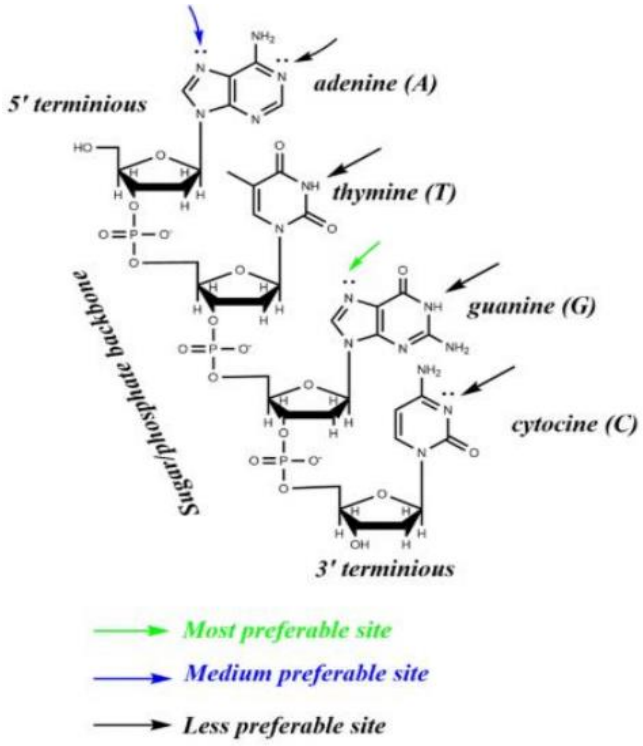

Figure 3.2: Cisplatin binding sites to DNA and respective order of preference. Obatined from:[16].

The formation of these DNA adducts causes the inhibition of the replication and transcription processes, cell cycle arrest and DNA repair. Once the adequate repairing is not successful, abnormal mitosis starts and activates the apoptosis pathways. There are multiple processes involved in apoptosis but they all coincide in a final and irreversible phase where cellular constituents are digested by the responsible enzymes [23]. Other

mechanism of action associated to Cisplatin action is the formation of reactive oxygen species (ROS) like hydroxyl radicals and superoxide that cause lipid peroxidation, reduction of sulfydryl groups and the alteration of other normal mechanisms, leading to DNA damage and apoptosis. ROS can also cause mitochondrial respiratory disfunction that facilitates the rupture of this organelle and the consequent release of substances that activate a group of caspases, cysteine proteases that play essential roles in programmed cell death [16].

For human treatment, Cisplatin administrated dose needs to be limited due to its toxicity to the renal, cochlear, vestibular and peripheral nervous systems [26]. The described combined therapy of surgery and chemotherapy is effective as first-line regime but 75% of ovarian cancer patients can experience recurrence, becoming more vulnerable to develop resistance to chemotherapy and eventually death [16]. Indeed, the acquired cell resistance to Cisplatin can arise after various exposures to this drug and is one of the major problems encountered during treatment plans. A decrease in drug accumulation in the cytoplasm or nuclei of the cells by degradation of cellular receptors, over-expression of detoxification compounds and increase in DNA repair are some of the possible mechanisms that are associated to resistant cells and disrupt their trace elements homeostasis [27].

Trying to overcome these limitations and in the search for Cisplatin analogues that would be more effective and less harmful for the patient, two platinum complexes Carboplatin and Oxaliplatin were developed and approved for clinical use [28].

Carboplatin has cyclobutanedicarboxylate as leaving group instead of chloride and demonstrates a lower toxic behavior and lesser side effects, allowing to apply higher doses to the patient and have better efficiency. In spite of these advantages, Carboplatin is active towards the same type of cancers as Cisplatin and inactive in cells that developed Cisplatin resistance, not being able to be used as alternative treatment [28].

On the other hand, Oxaliplatin is used in cases with higher resistance to Cisplatin as the case of colon cancer. This compound presents dicarboxylate as leaving group and 1,2-diamminocyclohexane in place of the two monodentate ammine ligands, that improve lipophilicity and the uptake through cell membrane. It presents a slightly different mechanism of action from Cisplatin, forming both inter- and intra-strand cross links in DNA, which prevent its replication and transcription, causing cell death [28].

To sum up, all the present platinum complexes have side effects that may require patients to be prescribed with dose reductions in their platinum drugs and extensive monitoring of their blood biochemistry, kidney and liver function [28].

3.3 Other Metal-Based Compounds

Several metals are essential biological elements involved in a variety of biological processes, from structural functions to enzymes co-factors. Metals like copper, cobalt, manganese, iron and zinc are present in trace concentrations and the balance between intracellular and extracellular concentrations needs to be maintained for the normal function of the body [29].

Because of their active participation in reduction and oxidation reactions, variable coordination modes (different oxidation states, coordination numbers and geometries) and reaction towards organic subtracts, metal-based complexes have an unlimited potential as cancer therapeutics [29, 30].

Complexes are chemical compounds based on the bond between a metal and a ligand that originate chemical entities with unique properties and different from the precursory species. The ligand and metal characteristics are of maximal importance when it comes to biological applications [31].

The discover of Cisplatin in the 60's constituted a milestone in the history of chemotherapy for introducing metal-based compounds in cancer treatment [29]. Other transition metal complexes have been receiving special attention. Transition metals are included in the "d"block of the periodic table, between the third and twelfth groups. The high electron affinity, number of electrons in the d shell and tendency to undergo redox reactions of these type of metals are some of the features that have impact in the biological action of their complexes.

The search for nonplatinum anticancer drugs that could result in lesser toxicity, more selectivity and a broader spectrum of activity, yielded a plethora of interesting compounds. A better understanding of their chemistry and mode of action may facilitate the development of anticancer drugs based on these compounds [32]. Metal complexes with ions like Cu, Co, Zn and Fe have been explored by the assumption that the use of endogenous metals would decrease cytotoxicity revealed by platinum complexes [29, 33, 34]. The requirement to develop a broad arsenal of drugs with high selectivity and fewer side effects, targeting one or more cellular components also lead to the development of a wide range of complexes such us those with the nobel metals Ag and Au, highlighting their important role in the inhibition of important vital enzymes involved in cancer cells growth and proliferation [35].

3.3.1 Copper Complexes

Copper complexes have attracted special attention for their redox activity and for presenting a less expensive alternative to the platinum drugs. Besides antitumor potential, copper complexes also have promising antimicrobial, antituberculosis, antimalarial, antifungal, and anti-inflammatory activity [34].

Copper is a transition and redox active metal, being able to shift between its reduced

(Cu^{+} , Cu(I)) and oxidized form (Cu^{2+}, Cu(II)). It acts as catalytic factor and structural constituent of many enzymes [36]. The homeostasis of this metal is fundamental for the good functioning of the organisms and is maintained by copper transporters (like CTR1 and ATP7A/B responsible for copper uptake, cellular distribution and efflux) and small molecules like glutathione and metallothioneins that act as detoxification agents [36]. It is also known that copper participates actively in healthy and carcinogenic ?? through diverse mechanisms. Cu ions stimulate the proliferation and migration of endothelial cells, control pro-angiogenic mediators synthesis and excretion and boost angiogenin's activity by establishing a direct bond to this molecule. This contributions allow the formation of new blood vessels by tumor cells, which enables tumor growth, invasion, and metastasis [36, 37].

This influence and accumulation of copper in tumor cells triggered intense investigations of copper complexes as anticancer therapeutics. They can be classified in copper chelators that capture copper ions within the cells and interfere with the mentioned cancer progression processes and copper ionophores, that are more effective in killing cancer cells by taking copper into the cells to ativate toxic pathways that lead to cell death [36].

The properties demonstrated by copper-coordinated compounds depends largely on the copper oxidation state, the complex structure, type of ligand and the donor atoms that participate on the bond [33, 37]. From the three stable oxidation states for copper, Cu(I), Cu(II) and Cu(III), the copper coordination chemistry is dominated by Cu(II) and some (but few) Cu(I) compounds.

An important aspect of the behavior of copper in coordination and physiological environment is the already mentioned Cu(I)/Cu(II) redox potential. The easiness in the Cu(I)/Cu(II) conversion by redox reactions has significant impact in the oxidation of organic substrates. As an example, the reactions between copper ions and reduced dioxygen derivatives (e.g., superoxide O^{-2}) are indispensable in Cu/Zn Superoxide Dismutase (SOD), an important enzyme that acts against oxidative stress caused by ROS, and may be part of the process of biological oxidative damage caused by copper [38].

Inside cells, Cu(II) is usually reduced to Cu(I) especially in cancer cells where the anoxic medium promotes this conversion. The redox potential associated to copper complexes widely vary according to the complex structure and interactions with the surrounding environment, e.g., in the oxidation of Cu(I) complexes when reacting to dioxygen register a range of potentials coming from -1.5 V to +1.3 V. [37]. When it comes to the mechanism of action, some copper complexes are associated to a SOD similar activity [37]. While others are responsible for increasing intracellular ROS levels that cause interference with the structure of proteins and with some enzyme pathways [37]. In fact, the majority of Cu(II) compounds bond with cellular glutathione and form a Cu(I) compound with the ability to induce the generation of superoxide anions that can induce ROS formation [34]. Other possible target for Cu complexes are DNA topoisomerases and proteasomes [37]. The first mentioned molecules are enzymes responsible for solving problems associated to chromatin processes (replication, transcription, recombination,

reorganization) and regulate gene activity by changing the state of DNA's supercoil. The second is a protein complex accountable for the degradation of intracellular proteins, and has been recorded Cu complexes activity to inhibit and disrupt proteosomes associated to essential proteins for the functioning of the cell cycle [37]. There has also been record of inhibition of telomerase activity, as well as DNA degradation and intercalation and induction of paraptosis [34].

3.3.2 Gold Complexes

Another class of metal-based complexes that have been studied are the gold complexes. These compounds have been associated to antimicrobial, anti-inflammatory, immunosuppressive and anticancer properties that can be promising for a more effective cancer treatment by minimizing secondary effects, chronic infections and increasing cellular uptake and selectivity towards cancer cells [39, 40]. In fact, some Au (I) and Au (III), when compared to Cisplatin, have presented better selectivity and efficiency towards cancer cells [41].

One of the most studied gold complexes is Auranofin, the reference compound for the development of new therapeutic gold-based compounds. Auranofin is a coordinated gold (I) complex that is commonly integrated in the treatment plans for rheumatoid arthritis and also revealed antimicrobial and antitumor activity. It was approved by the Food and Drug Administration (FDA) for several clinical trials to test its efficiency against multiple types of cancer such as leukemia and ovarian cancer. In spite of that, the fundamental mechanisms that originate the antitumor activity in ovarian cancer cells are not yet completely comprehended [40].

The mechanisms of action underlying the cytotoxicity of gold complexes is different from platinum-based compounds and usually involve the inhibition of enzymes, especially those with thiol groups in their structure. Considering this, the enzymes Thioredoxin Reductases (TrxR), glutathione reductases and cysteine proteases that contain thiol groups and are over-expressed in cancer cells are the most probable target for gold complexes in cancer treatment. The inhibitory action towards these enzymes can compromise the redox state of the cell and increase the production of ROS, leading to oxidative stress and apoptosis [40].

The stability of gold complexes in physiological environment, highly influenced by the nature of the associated ligand, remains a considerable challenge. For that matter, ligands with carbon, nitrogen, oxygen and specially, sulfur have been tested for their stabilizing effect, in particular, by preventing undesired intracellular redox reactions [42]. In fact, S. A. Sousa et al. [40] tested Au (III) complexes with sulfur donor atoms against ovarian cancer cells and all four complexes revealed promising results. It was measured high cytotoxic activity, ROS production and caspase 3/7 (enzyme involved in apoptosis) activation and no interaction with the DNA molecule.

3.3.3 Silver Complexes

For centuries, silver has been used for various medical applications, in the form of inorganic salts and complexes, mainly because of its antibacterial activity. The majority of reagents used, e.g. silver nitrate and silver sulfonamides, all have disadvantages (like high solubility in human serum that leads to dissociation and inactivation of the compound) that restrict their clinical usefulness. Considering this, its crucial that the active silver ions are firmly coordinated to adequate ligands that accentuate their most interesting properties [43].

Ag(I) complexes aroused great interest for displaying relevant antitumor properties. Some compounds revealed intenser anticancer activity and less cellular resistance development from that caused by Cisplatin and derivatives [35, 44]. A large variety of ligands has been associated to the structure of Ag(I) complexes but the ones that have been demonstrating the best results usually contain N-heterocycles (phenanthrolines, pyridines, and polypyridines, etc.), N-heterocyclic carbenes (NHC), and phosphines [45].

The mechanism of action of silver-based drugs has not been fully understood but there are records that indicate to involve the release of Ag ions that can enter the cell membrane and disrupt its function, by interfering with the topoisomerases activity [35, 43].

Aydin et al.[46] tested dicyanidoargentate(I) complexes that induced the apoptotic pathway in HT29 colon cancer cells, through the inhibition of Topo I DNA relaxation activity, interfering with DNA replication [35]. More recently, Rendošová M. et al. [47] assessed the biological behavior of a silver pyridine-2-sulfonate complex that besides its high antibacterial effect, was able to suppress L1210 leukemic cells growth, causing a necrotic and apoptotic effect by inhibiting Topo I at a concentration of 30 μM and interacting with DNA by partial intercalation [35].

Other possible biological targets have been identified and further investigation is necessary to extend the knowledge on the interactions between Ag(I)-complexes and both tumor cells and microorganisms [43]. The general cytostatic behaviour of silver complexes of inhibiting tumour growth without direct cytotoxicity is considerably well documented but the majority of the studies were performed *in vitro* conditions and only a few carried over to *in vivo* evaluation [43]. Some well-designed Ag(I) complexes become devoid of some or all of its activity initially demonstrated *in vitro* when transferred to *in vivo* conditions, due to the formation of insoluble AgCl or binding of the complex to cell enzymes. The most significant information on the effects of silver complexes on tumor growth were registered for ovarian cancer and lung carcinoma models, with relevant decreased growth [45].

3.3.4 Camphor-based Metal Complexes

The search for Cisplatin alternatives is based on a strategy that includes modifying the structure of existing platinum compounds, testing complexes with different transition

metals and including ligands that are natural and synthetic organic products [48]. The association of a metal core to a drug in use or with known therapeutic effects is expected to have a synergistic effect of the two components to improve the efficacy of the resulting complex [45].

Camphor ($C_{10}H_{16}O$, figure 3.3) is a natural compound that has been used for its numerous pharmacological effects: antimicrobial, anesthetic, anti-inflammatory, antibacterial, and others [49, 50]. Due to its high lipophilic properties, camphor enters the cell membranes and is specially well absorbed by mucous membranes and gastrointestinal tract. Considering this, presents a high volume of distribution, i.e., has propensity to leave the plasma and enter the extra-vascular compartments of the body. In spite of all associated benefits and pharmacological applications, Camphor is highly toxic. Doses superior to 30 mg/Kg cause toxic reactions in multiple tissues and organs therefore its clinical usage of camphor is restrictive [51].

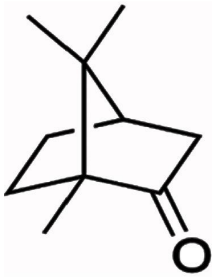

Figure 3.3: Camphor chemical structure. Obtained from: [9]

The camphor advantageous action on cancer treatment when combined with cytotoxic agents has been reported in multiple studies with promising results [52].

Cardoso J.M.S. et al. [2], tested silver (I) camphorsulphonylimine complexes against the human ovarian cancer cells A2780 (sensitive to Cisplatin), A2780 cisR (resistant to Cisplatin) and non-tumoral embryonic kidney Human Embryonic Kidney (HEK)293 cells. The tested complexes demonstrated higher activity than Cisplatin against ovarian cancer cells. On the other hand, the ligands isolated from the complex structure, demonstrated no significant cytotoxicity. Following these results, the ability to bond to the DNA molecule was assessed using Calf Thymus Deoxyribonucleic Acid (CT-DNA) and fluorescence techniques. The results revealed that all the complexes possibly bonded to DNA by different mechanisms (two of them by intercalation and the third was unclear/unknown). It was also possible to establish a cause-effect relationship between a higher binding ability and a higher cytotoxic effect. The excessively high cytotoxicity against healthy cells (HEK293) is the principal obstacle for a potential therapeutic use of these compounds.

A more recent study [48] also tested silver complexes with camphor carboxylate and camphor carboxamides ligands. The most relevant result was obtained for one of the silver camphor carboxylate complexes that demonstrated higher cytotoxicity than Cisplatin towards A2780 ovarian cancer cells and A2780 cisplatin resistant (A2780cisR) but showed

low toxicity against the non-tumoral human embryonic kidney (HEK293) and hence, a significant pharmacological selectivity towards ovarian cancer cells. The redox properties of these compounds, that are susceptible to be reduced, are directly associated to their anticancer properties by oxidation of biological substrates, interfering with the normal redox energy generation processes.

Testing a different transition metal, Petrović A. et al. [53] synthesized rodium(III) complexes with camphor-derived Bis(pyrazolylpyridine) ligands. This complexes were analyzed by Ultraviolet-Visible (UV-Vis) and emission spectral studies that revealed that theses compounds bonded easily with CT-DNA and bovine serum albumin. When performing cytotoxicity tests, complex represented in figure 3.4 demonstrated efficiency against human epithelial colorectal carcinoma cells.

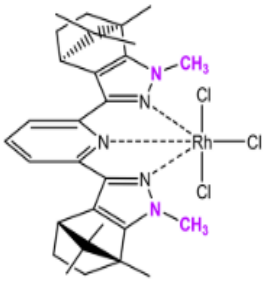

Figure 3.4: Rh(III) complex that revealed significant efficacy against human epithelial colorectal carcinoma. Obtained from: [53]

Fernandes T.A. et al. [50], evaluated the cytotoxicity of three synthesized polynuclear Cu(I) camphor complexes against human colon carcinoma HT29. All the complexes demonstrated variable cytotoxic activity due to the influence of the different ligands and co-ligands. One of the most active compounds reached cytotoxic values similar to Cisplatin while, the camphor compounds used as ligands did not demonstrate any significant activity towards the cells. Copper cellular uptake was assessed by ICP-MS for HT29 cells treated with the complexes that presented low, moderate and higher activity. The obtained results were not representative of the activity of the complexes, I.e., it was not possible to establish any correlation between the Cu uptake by the cells and the intensity of the associated cellular viability decrease. The interactions with potential cellular targets (more or less sensitive) were the main reasons associated to these findings. It was also proposed that the polynuclear complexes would just act as carriers to take the active camphor compounds to the cells and would suffer the loss of CuCl once inside the cell to form unsaturated intermediates with less copper and higher affinity to receptors and biological interactions.

Later, Kokina et al. [54] also performed comparative studies of zinc(II), palladium(II), and copper(I) chlorides with camphor thiosemicarbazone ligands agains the breast cancer cell line MCF-7. This team discovered that the Cu(I) complexes where more cytotoxic

than the mononuclear Zn(II) and binuclear Pd(II) complexes. The complexes presented more activity than Cisplatin and the ligands isolated, once again, did not had any toxic effect towards the cells.

3.4 Contribution of Imaging Techniques in Unraveling New Metal-Based Drugs

The continuous evolution of the proton probe optics and reduction of the beam dimensions led to a progressively improved image resolution. The morphological images and elemental distribution maps that are obtained through STIM, and PIXE and EBS, respectively, are very useful to study the distribution profiles of metals in whole single cells to evaluate the cellular uptake of metal-based drugs [15]. Indeed, these techniques have become indispensable for important discoveries in the biological and biomedical field, by allowing the visualization of cellular and subcellular processes in whole cells (normally with sizes between 10 and 100 μm) [40].

First investigations on single cell imaging using nuclear microscopy date back to 1995. Moretto P. et al. [27] proved the potential of nuclear microscopy techniques to analyze the individual response of cells to a pharmacological stress. They proceeded to the *in vitro* incubation of two different ovarian cancer cell-lines, sensitive and resistant to Cisplatin, with this drug in pharmacological concentrations. After the treatment, PIXE with EBS and STIM mapping were performed. The subcellular elemental resolution attained with this method allowed to visualize an homogeneous distribution of platinum within whole cells of both cell lines, confirming the Cisplatin binding to numerous intracellular sites, in the cytoplasm and in the nucleus. The authors also showed changes in the cellular distribution of physiological elements following Cisplatin treatment, such as small accumulations of iron (as seen in figure 3.5) localized in nuclear and perinuclear areas.

In 2017, Ribeiro et al. [55] studied the activity of Copper(II) complexes with Schiff bases ligands, derived from pyrazolyl against MCF7 breast and PC3 prostate cancer cell lines. The cellular uptake of copper was assessed using nuclear microscopy in selected complexes that showed relevant activity. The STIM density maps enabled to correlate the PC3 cell morphology (ovoid chape and condensed central core) with the elemental distribution maps of P, K, Ca and Cu (figure 3.6). While in control PC3 cells, the presence of Cu was residual, the cells incubated with the compound at 20 μM and 200 μM showed a dose dependent uptake of Cu, which preferentially accumulated in nuclear and perinuclear regions. Therefore, direct imaging of Cu in single cells demonstrated the ability of this complex to cross the cell membrane and highlighted that the cellular uptake of Cu may interfere in the homeostasis of physiological elements involved in membrane potential maintenance.

More recently, Dominelli B. et al. [56] tested dinuclear Au(I) complexes bearing 2-hydroxyethane-1,1-diyl-bridged bisimidazolylidene ligands. One of the complexes

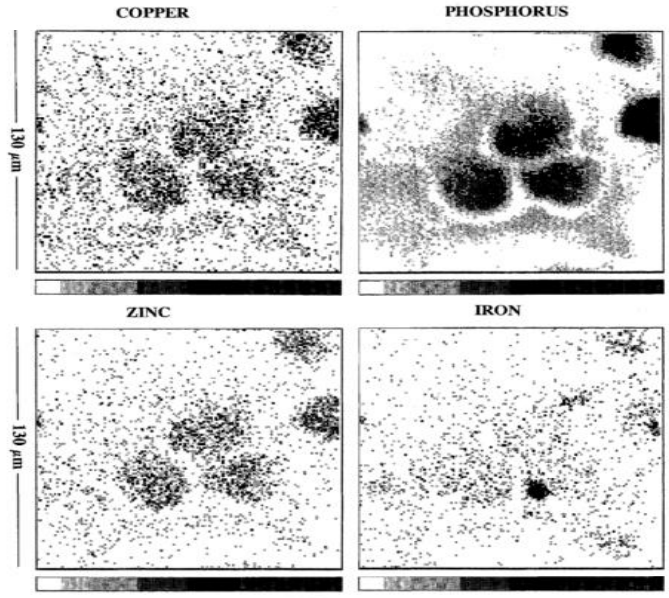

Figure 3.5: Phosphorus, iron, copper and zinc distribution maps in a Cisplatin-resistant treated with Cisplatin. An iron accumulation is visible on the right bottom image, by an intenser coloration of black inside the cellular area. Obtained from: [27]

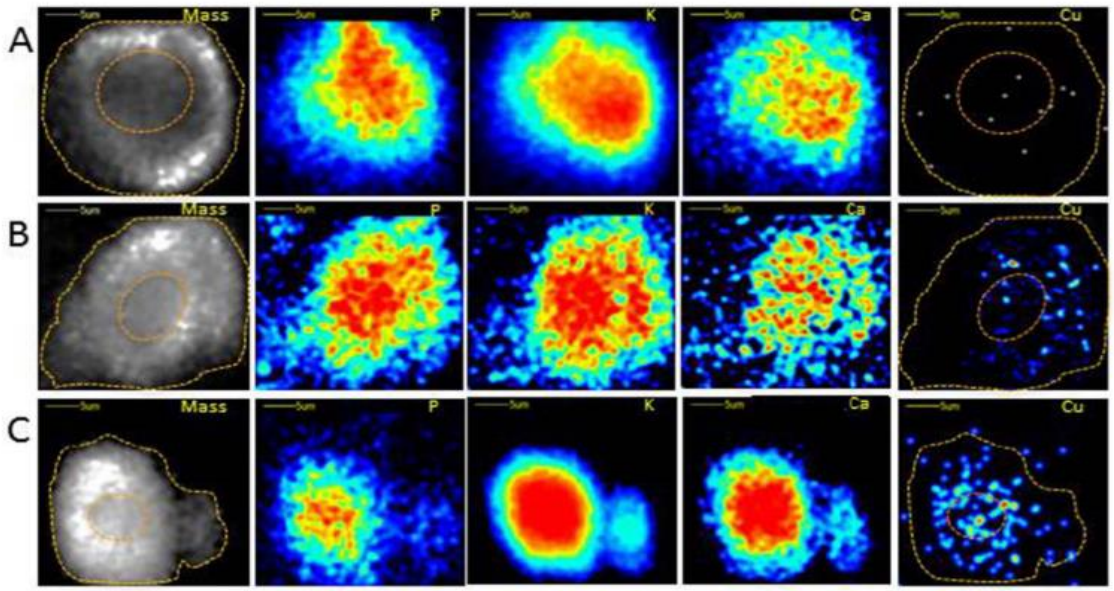

Figure 3.6: Density and elemental maps of P, K, Ca and Cu distribution in individual PC3 cells under control (A), 20 μM (B) and 200 μM (C) of the Copper(II) complex with Schiff base ligand in study. The dotted lines in mass and Cu maps indicate the cytoplasm and nuclear limits. The mass density and elemental distributions are represented by a color gradient with a dynamic scale: high level — red, to low level — black/dark blue. Obtained from: [55]

showed promising characteristics, such as considerable toxicity against several cancer cell lines (breast, ovarian and prostate) with better results than Cisplatin inclusively in A2780cisR (Cisplatin resistant) and promising selectivity, as less toxicity was observed toward a healthy cell line hamster lung fibroblasts (V79). By analyzing the EBS spectra to extract the energy loss of protons thru the cell, it was possible to reconstruct a 3D cell model (figure 3.7) with five layers in depth revealing that Au is mainly located in the cell core, where organelles (e.g., mitochondria) and membrane systems are. Therefore, combining nuclear microscopy data with complementary techniques it was possible to propose as a possible mechanism of action for the complex the interaction with mitochondria membrane, by the inhibition of TrxR activity, a key mitochondrial antioxidant enzyme, that leads to ROS accumulation and eventually mitochondria dysfunction.

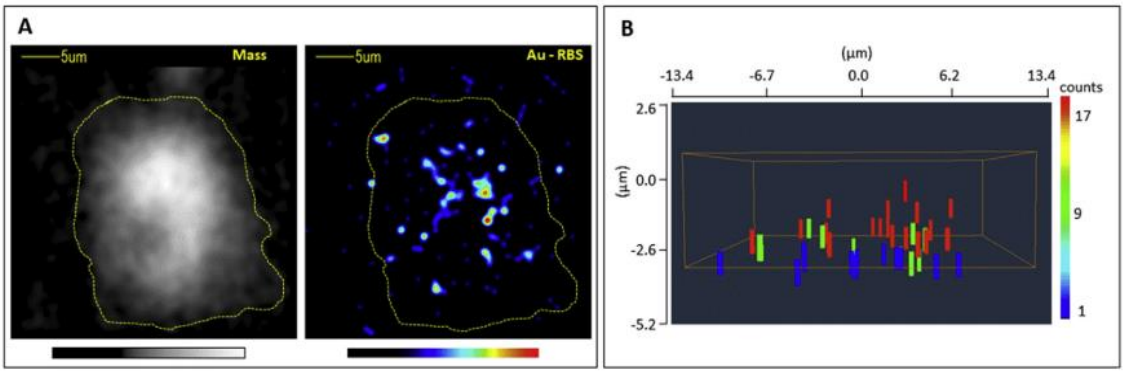

Figure 3.7: (A) Nuclear microscopy images of mass density (Mass) and Au distribution obtained from the RBS spectrum of a PC3 cell incubated with the Au(I) complex in study. (B) 3D representation of the distribution of Au in the cell depicted in (A). Obtained from: [56]

In the same year, Jakob C. et al. [57] evaluated the biological behaviour of Au(I) *bis*-NHC complexes, reaching promising results for two complexes: one containing ester and the other, amide in its structure. Cisplatin comparable results were obtained for these complexes that presented activity towards the Cisplatin resistant cell line. The PC3 cells treated with both complexes at equal concentrations were analyzed to nuclear microscopy techniques and the results showed that the compounds have different distribution profiles. The presence of gold in the cells treated with the complex containing ester was almost non existing, indicating that the drug was weakly connected to the cell surface, and for cells treated with the second compound in study, the Au distribution was visibly disperse but indicative of cellular uptake. In spite of that, morphological alterations and imbalance of elements essential for biologic processes suggest that the cellular effects were more significant for the compound containing ester.

Another method to study the intracellular distribution of trace elements and therapeutic metal complexes is synchrotron radiation X-ray fluorescence microscopy (SR-XRF),

based on the analysis of the characteristic X-rays emitted from the sample that is irradiated with high-flux X-rays beam at a synchrontron facility. The emergence of third-generation synchrotrons turned SR-XRF in one of the most versatile methods to imaging hydrated biological specimens and whole cells with spatial resolutions < 300 nm and high sensitivity for elemental detection. Due to high-flux beam delivered in SR facilities, energy tuning is possible what is appropriate to optimize the determination of the oxidation state and coordination environment of metal cations [12].

There are reports of the use of this technique for the *in vitro* and *ex vivo* study of metal-based anticancer drugs containing platinum, ruthenium, iridium, osmium, and others. As XRF is a multi-elemental technique, like PIXE, it is also possible to assess the endogenous elements in cellular homeostasis. For instance, the importance of zinc was revealed in the resistance of the cells to Cisplatin an in the biological response of cells against gadolinium complexes with triphenylphosphonium ligands with high affinity to mitochondria [58].

Wedding J. et al. [59], studied the stability and intracellular distribution of a rhenium(I) complex with ligands containing iodine in 22Rv1 human prostate carcinoma cells using SR-XRF imaging. The distributions of rhenium and iodine in the cells were correlated suggesting that there is no dissociation of the ligand from the complex structure. The preferential localization of the complex was associated to nuclear and perinuclear regions of the cell that caused cellular homeostasis unbalance.

Recently, Bolitho et al. [60] combined high-resolution X-ray imaging methods to study the efficiency of two photoactivatable Pt(IV) complexes in single PC3 cells. An efficient cellular uptake was visualized with SR-XRF, associated with low toxicity. Upon photoactivation, serious and concentration-dependent damage was caused to the treated cells, like cell shrinkage and specific organelle damage.

The SR-XRF technique provides cellular imaging with higher resolution and elemental sensitivity than the results obtained with PIXE in nuclear microscopy routine experiments, but the results are only qualitative. In addition, the synchrotron facilities have massive dimensions when compared to particle accelerators used in nuclear microscopy. There are few synchrotrons available in the world with nano-XRF possibilities, what limits the access and sometimes the adequate continuity of experiments.

4

Materials and Methods

4.1 Biological Assays

4.1.1 Cytotoxic Activity (MTT Assay)

The cytotoxic activity was evaluated in the human epithelial ovarian cancer cells Cisplatin sensitive A2780 (Sigma-Aldrich) and OVCAR3 (American Type Culture Collection (ATCC)) and also, in healthy human dermal fibroblasts, Human Dermal Fibroblasts (HDF) (Sigma-Aldrich) and hamster lung fibroblasts, V79 (ATCC). These cells were grown in Roswell Park Memorial Institute (RPMI) 1640 medium (ovarian and V79 cells) supplemented with 10% FBS or fibroblast growth medium (HDF cells) and maintained at 37ºC, 5% CO2 and humidified atmosphere in an incubator (Heraeus, Germany).

Cell viability was assessed by the MTT assay, after the cells being submitted to treatment with the compounds [61, 62]. The yellow-colored tetrazolium salt MTT is reduced to nonwater-soluble purple formazan crystals (figure 4.1) by succinate dehydrogenase system of the active mitochondria and by the co-enzyme Nicotinamide Adenine Dinucleotide + Hydrogen (NADH) (reduced form), only present in the viable cells.

Cells were seeded in 96-well plates at a density of 10^4 cells per well in 200 μL medium and allowed to adhere overnight. After, the medium was discarded and 200 μL of fresh medium containing each compound in the concentration range 10^{-7} M to 10^{-4} M was added to the cells for 24h treatment. Complexes were first dissolved in Dimethyl Sulfoxide (DMSO) and then in medium to prepare the serial dilutions.

After 24h incubation, the solutions were aspirated and 200 µL of MTT solution (0.5 mg/ mL) were added to each well. After 3 h at 37 ºC, the MTT solution was aspirated and the formazan crystals formed were solubilized with DMSO. The absorbance at 570 nm (maximum of the absorbance spectrum of formazan) was measured using a plate spectrophotometer (Power Wave Xs, Bio-Tek). The obtained intensity values are proportional to the number of viable and metabolically active cells. At least four replicates for each concentration were analysed and the results are presented in chapter 5 as the mean of the obtained values (MEAN) and the associated Standard Deviation (SD).

The IC_{50} (half-minimal inhibitory concentration) values, indicative of the necessary

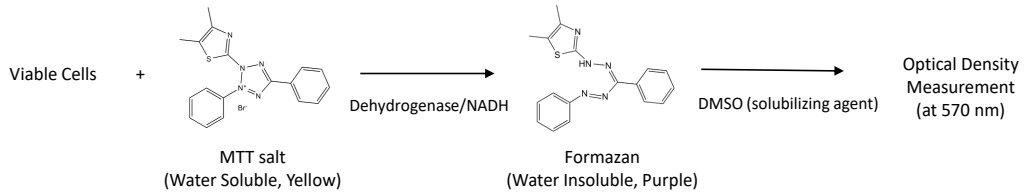

Figure 4.1: Conversion by viable cells of MTT to formazan crystals and respective solubilization to proceed to optical density measurement. Adapted from: [40].

concentration of the complex to exert half of its maximal inhibitory effect, were calculated from dose-response curves (appendix C) using the GraphPad Prism software (vs. 5.0). This value is representative of the cytotoxic activity of the tested compounds: the lower IC_{50} value, the more cytotoxic the complex is. The metal precursors of the complexes were also tested using the same method but only applied to the OVCAR3 cells. The concentrations of the prepared solutions are analogous to the ones used with the correspondent complex of the precursor in study.

4.1.2 Stability in Physiological Media (UV-Vis Spectroscopy)

All the biological studies for this dissertation are carried out in aqueous media at physiological pH. These conditions are ideal for certain reactions (e.g. redox reactions) to happen and alter the initial chemical structure and properties of the compounds. Therefore, it is necessary to ensure that the complexes do not precipitate in the aqueous milieu and that they are stable in the timescale of the studies.

The stability in cellular medium of the complexes (1 to 9) was evaluated for 48 hours using UV-Vis spectroscopy that is based on the recording of the absorption by the sample of radiations in the ultraviolet (10 to 400 nm) and visible regions (400 to 800 nm) of the electromagnetic spectrum [40]. The absorbed radiations have characteristic intensities and wavelengths/frequencies that may suffer alterations over time or for different mixture compositions and in that case, it is indicative of instability of the complex in study [63].

The spectrophotometer Agilent Technologies Cary 60 and the Cary WinUV Software (figure 4.2) allowed the record of an absorption spectrum for each complex dissolved to obtain three different mixtures: DMSO (1%) as a reference, in DMSO (1%) and colorless Dulbecco's Modified Eagle Medium (DMEM) and finally in DMSO (1%), colorless DMEM and Fetal Bovine Serum (FBS) (10%). In order to get comparable values between the different compounds, each mixture presented the same concentration of the different complexes.

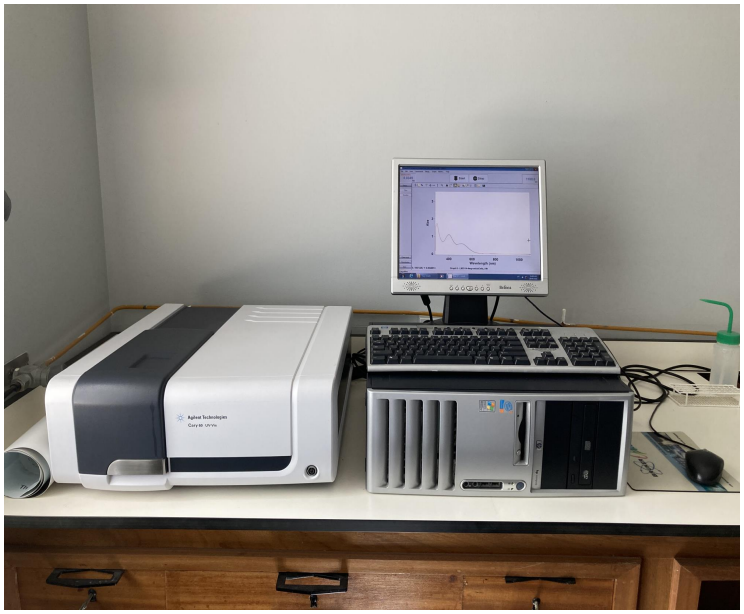

Figure 4.2: Experimental setup used to evaluate the complexes' behaviour in solution. The spectra were obtained using an Agilent Tecchnologies Cary 60 UV-Vis device and the correspondent software, Cary WinUV Software.

The obtained spectra represent the intensity of the absorbed radiations versus their wavelength, representing the essential data for a merely qualitative analysis of the stability of the compounds in physiological media.

4.1.3 DNA interaction (Agarose Gel Eletrophoresis)

Another common mechanism of action of many anticancer drugs (like Cisplatin) is through interaction with the DNA molecule, preventing the uncontrolled cellular division [64]. Therefore, the DNA binding activity of the metal complexes was assessed through their ability to alter the electrophoretic mobilities of the Covalently Closed Circular (ccc) and Open Circular (oc) forms of ϕX174 supercoiled DNA, as previously described [40].

The different forms of DNA move with different migration speeds and a depletion in the rate of migration through the agarose gel is observed when a compound unwinds the DNA double helix – the reduction in the number of supercoils results in a density of ccc DNA decrease. In that case, increasing the molar ratio of complex per nucleotide (ri), decreases the rate of migration of ccc DNA until it comigrates with oc DNA and reaching a coalescence point where all DNA's supercoils are removed [64, 65]. That result can be observed for Cisplatin as can be seen in figure 4.3.

To perform the assay, each tested mixture was prepared containing 200 ng of ϕX174 DNA (Promega) and different concentrations (0.5, 1, 5, 10 and 15 μM) of the complexes 1, 4, 5, 7, 8 and 9. The concentrations were chosen in order for the results to be comparable with the results previously described for Cisplatin. After incubation for 24 h at 37 °C, in the dark, the samples were run in a 0.8% agarose gel in Tris-acetate-EDTA (TAE) buffer

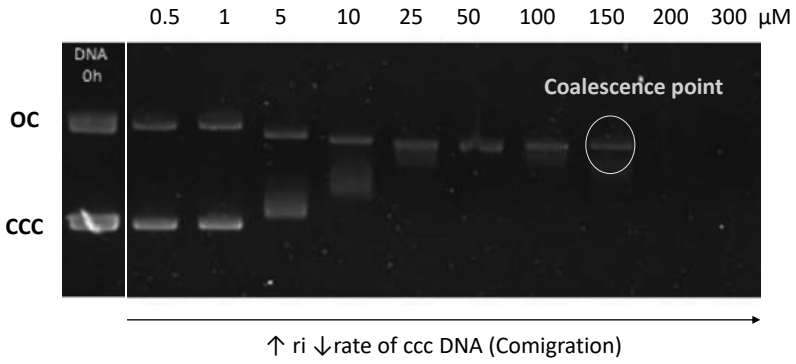

Figure 4.3: Agarose gel electrophoresis result for Cisplatin used as a reference for comparison with the images acquired for the copper, silver and gold complexes. The described effect of the increasing ri on the rate of migration is clear and the coalescence point can be identified at 10 μM. Adapted from: [65].

for 3h at 90 V. The gel was then stained using a 3× GelRed® (Biotium) solution in H_2O and imaged in an AlphaImagerEP (Alpha Innotech). The obtained images for the samples in study were always compared with the non-incubated plasmid and plasmid incubated with DMSO both used as control samples.

4.1.4 Detection of ROS (H_2DCF−DA Assay)

Cisplatin and other anticancer drugs induce the formation of ROS and sequentially activate cell death mechanisms, inducing apoptosis [61]. To evaluate the induction of intracellular ROS levels, mainly peroxides, by the complexes, the dihydro-2'7'dichlorofluorescein diacetate (H_2DCF−DA) assay was used for its high sensibility to the reactive species in study. This H_2DCF−DA cell-permeable molecular probe is de-esterified within the cell and turns to highly fluorescent 2',7'-dichlorofluorescin (DCF) upon oxidation with ROS (figure 4.4).

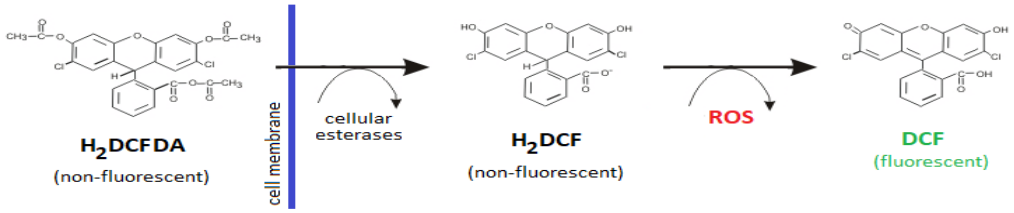

Figure 4.4: The fundamental principle for ROS level measurement by the H_2DCF−DA assay: the 2´,7´-dichlorofluorescin diacetate (H_2DCF−DA) probe is a non-fluorescent molecule that enters the cell and suffers deacetylation by cellular esterases to a non-fluorescent 2'7'-dichlorofluorescin (H_2DCF). H_2DCF then oxidatised by ROS to generate a highly fluorescent 2',7'-dichlorofluorescein (DCF). Obtained from:[66].

For the assays, OVCAR3 cells (2×10^4 cells /well) were seeded in 96-well plates and

left to grow and adhere overnight. After, the medium was replaced with a solution of 10 μM H_2DCF−DA in colorless DMEM (FluoroBrite™ DMEM, Gibco®) and cells were incubated at 37°C for 30 min. Then the medium was aspirated and cells were incubated with the compounds in fresh medium for 1 h at selected concentrations of 10, 20, 50 or 100 μM for each copper complex, 0.1, 1, 10, 20 μM for each gold complex and 1, 10, 20 or 50 μM for each silver complex. Hydrogen peroxide was also included in the analysis as positive control. The incubation period was shorter than for the MTT assay due to the chemically reactive character of ROS. The concentrations used in the assays were selected taking into consideration the IC_{50} values of the complexes previously obtained.

DCF fluorescence was measured at an excitation wavelength of 492 nm and 517 nm of emission using Varioskan Lux multimode microplate reader (ThermoFisher Scientific). Results of fluorescence were expressed as the mean (of three replicates) fold change in fluorescence levels in relation to untreated OVCAR3 cells.

4.1.5 Generation of Superoxide Radicals (NBT assay)

The Nitro Blue Tetrazolium (NBT) assay was carried out based on a previously described method [61]. This assay was used to determine the ability of cells to produce superoxide anion $O_2^{\bullet -}$ (another ROS species), upon treatment with the compounds. NBT is a tetrazolium salt like MTT that crosses the cell membrane and suffers reduction by superoxide radical anion, resulting in dark blue NBT formazan particles.

A pre-treatment was effectuated to OVCAR3 cells (seeded into a 96-well plate) were treated with the complexes in medium for 1 h at 37°C at concentrations equivalent to the IC_{50} values (50 and 100 μM for the copper complexes 1, 2, 3 and 4; 20 and 50 μM for complexes 5 and 7; and finally, 10 and 20 μM for the most active complexes 6, 8 and 9). After that period of incubation, 20 μL of a NBT solution 10 mg/mL in water was added to the cell´s medium and incubation was subsequently prolonged for more 1 hour at 37°C. Then, the medium was discarded and the blue formazan particles were dissolved in 200 μL of 90% DMSO (90% DMSO: 10% NaOH 0.1 N with 0.1% SDS). The absorbance of the resulting NBT formazan was measured at 560 nm with a plate spectrophotometer. Each concentration was tested with at least six replicates and the results (mean ± SD) are expressed as % in relation to controls (untreated cells).

4.1.6 Lipid Peroxidation (TBARS Assay)

ROS are produced by multiple cellular processes but their levels can be increased in response to different stimuli. Normal cells can maintain oxidative homeostasis owing to the activity of various antioxidant systems that control ROS production through metabolic and signaling pathways. Upon a prolong increase in ROS levels, the antioxidant defense mechanisms can promote cell death [67]. ROS can react with the polyunsaturated fatty acids of lipid membranes and induce lipid peroxidation. The end products of lipid peroxidation are reactive aldehydes, such as malondialdehyde (MDA) that have been considered

to be a second messenger of the oxidative stress. Increased ROS level can inhibit tumor cell growth. Indeed, in tumors in advanced stages, a further increase of oxidative stress, such as that occurs when using several anticancer drugs can overcome the antioxidant defenses of cancer cells and induce apoptosis [67]. The MDA level is commonly used as a biomarker for lipid peroxidation [68]. In this study, the content of MDA in lipid extracts of OVCAR3 cells exposed to complexes 1, 5, 8 and 9 (complexes that demonstrated the most significant dose-dependent ROS production) was measured using a colorimetric kit (BioVision, CA, USA), a method that relies on the reaction of MDA with Thiobarbituric Acid (TBA) and the detection of the respective reactive products [61].

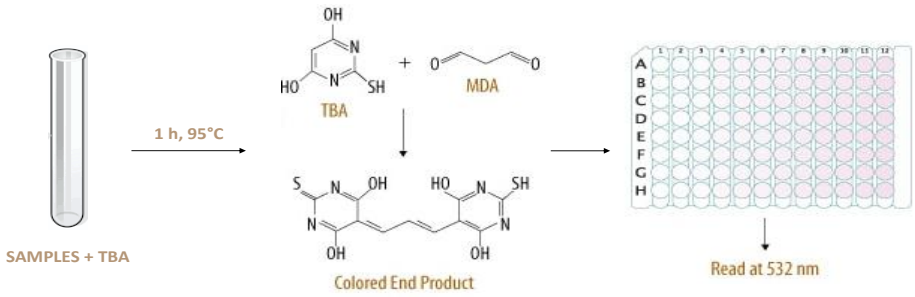

Figure 4.5: The principle for the lipid peroxidation detection assay. To the previously treated samples/standards is added the TBA reagent that reacts with MDA during incubation, producing a colored end product (MDA-TBA). Then, 200 μL of each mixture are placed in a 96-well plate to measure the absorbance at 532 nm, with the intensity values corresponding to the level of lipid peroxidation in the sample. Obtained from:[69].

Briefly, OVCAR3 cells (5×10^5 cells/2 mL medium) were seeded in 6-well plates and left to adhere for 24 h. Then, after treatment with the complexes at selected concentrations (100 μM for complexes 1 and 5; 20 μM for complex 8 and complex 9). The incubation period was 24 h at 37°C. After that, the medium was removed, the cells were washed with Phosphate-Buffered Saline (PBS), tripsinized and centrifuged. The cell pellet was treated following the kit recommended protocol. Then, the cells were lysed and centrifuged to remove insoluble materials. To 200 μL of the supernatant was added to 600 μL of TBA to generate the red-pink MDA-TBA adduct (Thiobarbituric Acid Reactive Substances (TBARS)) by incubating the mixture for 1 h at 95°C. After that, 200 μL were taken and transferred to a 96-well plate for MDA quantification at 532 nm. To generate a MDA standard curve (appendix B), MDA standards were processed in parallel with the samples, using the same procedure. This curve and respective equation was used as reference and allowed the association between the absorbance values of the studied samples with their MDA content value. Results were expressed as mean ± SD from the four replicates for each concentration.

4.2 Cellular Uptake

In order to understand the complexes' effectiveness (or lack of it) in the cells, the metal uptake was evaluated. This was done using the Ion Beam Analysis (IBA) techniques performed in the 2.5 MeV Van De Graaff accelerator installed at the *Instituto Superior Técnico* (IST)/*Campus Tecnológico e Nuclear* (CTN). The Van De Graaff accelerator is the key element for the whole setup since it is responsible for accelerating a proton beam to the desired energy, maintaining the beam current stability and its low energy spread (less than 100 eV per MeV) [6]. The trajectory of the accelerated ions is conditioned by the switching magnet that allows the selection of one of the three available beam lines where the various sample stages are installed. Both PIXE line and the central line that leads to the Nuclear Microprobe were used in this dissertation. The whole system of lines and chambers are kept in vacuum ($< 10^{-6}$ mbar). The technical details of the used devices and applied procedures are described in the sections bellow .

4.2.1 CTN Nuclear Microprobe

The central beam line that leads to the microprobe is the one where the verified energy dispersion of the beam is lower. All its components are represented in figure 4.6 and are described in this section.

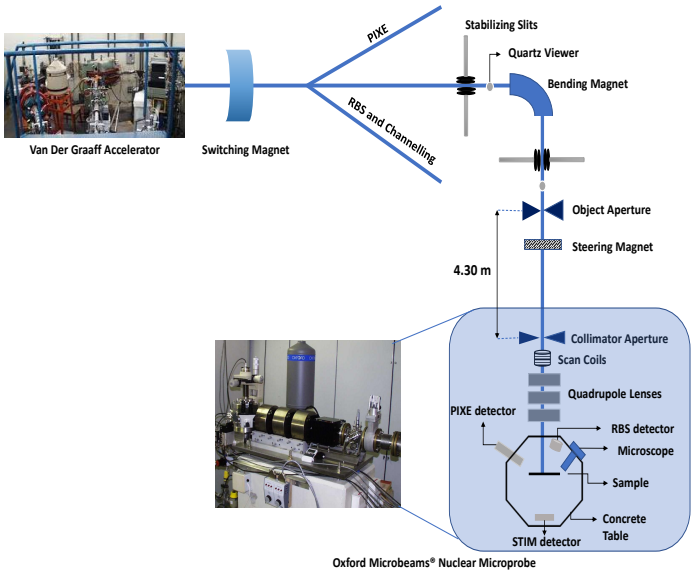

Figure 4.6: CTN/IST nuclear microprobe system, respective components and setup. Starting with the Van De Graaff accelerator, the beam line terminates with the Oxford Microbeams® nuclear microprobe sample stage where the samples are placed to be irradiated and analyzed. Adapted from: [70].

After the switching magnet, the accelerated protons firstly encounter the stabilizing

slits that are responsible for controlling the stability and the direction of the beam, ensuring that it is parallel to the beam line. The quartz viewers, present in more than one place in the beam line, allows the user to ensure the ideal conditions of transmission and focusing of the beam by obtaining visual contact with it and evaluating its behaviour. When reaching the 90º bending magnet, the beam is submitted to a magnetic field that selects the ions with a defined mass and energy. After the beam passes through another stabilizing slits and quartz mirror, it reaches the object and collimator apertures. The object aperture defines the beam area and the collimator aperture limits its divergence before entering the probe-forming lens system. Between these two elements, a steering magnet can also be found. Its function consists in enhancing the beam intensity and correcting beam trajectory changes caused by alterations of the charged particles in use, the beam energy or even by movements of the beam line structural components, without needing new mechanical alignment [8].

The Oxford Microbeams® nuclear microprobe also includes the scanning coils system, the quadrupole lenses focusing system and finally, the vacuum chamber that accommodates detectors and the sample stage.

The scanning coils system enables to scan the beam over the sample surface in 256x256 steps (pixels) to generate two-dimensional (2D) images from the spectral data collected [8].

Immediately before the vacuum chamber, a focusing system composed by a magnetic quadrupole triplet demagnify the beam to form a micrometre dimensions probe, which in routine analysis is of the order of 3x4 μm^2.

With an octagonal cylinder shape with ports on the flat faces, the final element of this beam line is the vacuum chamber. The samples are fixed to a support that is connected to the top base and are perpendicularly irradiated by the beam. To help place the samples and during the beam focusing operation, a stereo zoom microscope can be found in one of the lateral faces at a backward angle of 45°. All the microprobe components described until now are set in a concrete table on top of a polystyrene surface to decrease the effect of the vibrations coming from the ground and equipment that can influence the spatial resolution of the beam.

The detector used for the detection of X-rays emitted by the sample after the interaction with the accelerated protons (PIXE) is a silicon drift detector (SDD) with 30 mm^2 active area, positioned at 45° relative to the sample in the plane of the beam direction. The backscattered particles (EBS) are collected with a Si surface barrier detector with 200 mm^2 of approximately 20 keV resolution positioned at a backward angle of 40° with the beam direction. For STIM, a Si PIN diode behind the sample in off-axis angle of ~20° is used to detect the transmitted ions [8].

4.2.1.1 Maps Construction

For the construction of the elemental distribution maps, the detectors signals are recorded and each detected event is associated to a digital x and y position, determined by the scanning movement of the beam, i.e. the maps are obtained from the spectral data in each pixel. The consolidation of this information is done by commercially available code and results in maps with elemental distributions represented by a dynamic gradient of color. The 2D images of the sample enables the visualization of whole single selected cells and respective elemental distribution but it is also possible to select isolated details and specific zones of interest [6].

The 256x256 pixels PIXE and EBS maps that represent the scanned area are always informative about a specific selected element distribution on that region while STIM is indicative of the density of that area. As it was mentioned, the maps were built taking the detected events for the selected element or energy region in the spectrum as a reference. As an example, to obtain a map of Cu, the energy interval around copper characteristic Kα X-rays lines (maximum intensity at 8.028 KeV) in the PIXE spectra is selected. If the detected X-ray energy fits into the defined range, one count is added to the Cu map in the (x,y) position corresponding to the beam localization in the defined scan size. Therefore, the resulting images show the collected events originated by the interaction of the protons with Cu atoms and consequently, the Cu distribution and amount in the cell contained in the scanned area, visualized using a dynamic colour scale. The same process can be done to every element in the PIXE spectra and for the collected spectra (I.e., EBS and STIM) [8].

By extracting energy intervals from the STIM spectra enables discriminating regions of different mass density. This is useful to identify structures at the subcellular scale, such as the nuclear dense region from lower density cytoplasm. In figure 4.7, a STIM spectra corresponding to a scan over a sample region with a cell is displayed. Three layers were selected to illustrate how energy regions can be interpreted. The layer on the left correspond to the energy interval where particles crossing the samples suffered more energy loss thus representing denser regions of the sample. In the corresponding map, it is possible to identify a denser region (higher intensity colour) consistent with the nuclear region of the cell. The middle layer enabled to delineate the cellular contour and an average energy loss that associates with the cell cytoplasm. The layer at the right correspond to the most energetic protons, meaning those that passed through the sample with a small energy loss. This layer mostly represent the interactions of the proton beam with the silicon nitrate membrane, which has a thickness of 100 nm (it is possible to identify the cell location through the low intensity colour in the center of the map).

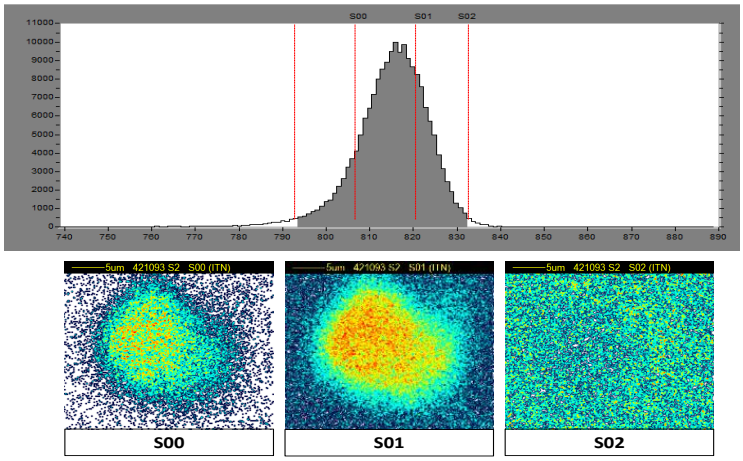

Figure 4.7: STIM spectrum and respective three maps of counts associated to the three defined energy intervals. S02 images a layer of the sample with minimum energy loss, S01 represents a medium energy layer where the cell contour is distinguished and S00 is the layer corresponding to the regions of the sample where protons lost more energy.

4.2.2 Imaging Elemental Distribution in Cells

About 10^6 OVCAR3 cells were were seeded on silicon frames using a 6-well plate to be analyzed by nuclear microscopy techniques. The handled silicon frames composed by 5x3 windows with an area of 0.56 mm^2 each and covered with a 100 nm silicon nitride membrane, were sterilized under an Ultraviolet (UV) light before use. Control and cells treated with the IC_{50} concentrations of the complexes 1 and 2 were incubated for 24h. Once the incubation period was over, the medium was removed and its remains were washed out with cold PBS. The frames with adherent cells were quench frozen and stored at -80°C. Before analysis cells were transferred to a cryostat and allowed to dry at -25°C overnight. This procedure preserves cells close to the *in vivo* condition. The frames were previously inspected under an optical microscope to identify the best regions of interest and cells to analyze. The elemental distributions and cell density images of whole cells were obtained by nuclear microscopy techniques (PIXE, EBS and STIM, respectively) as previously described. A proton beam with 2.0 MeV of energy focused to 2x3 μm^2 was scanned over the selected cells or regions of interest. The PIXE, EBS and STIM spectra were collected simultaneously. The position and spectral data collected in each pixel (256x256 pixels) was used to construct the maps that represent the scanned area. For PIXE, the most intense characteristic X-rays (usually Kα lines) of the various elements detected were used. For EBS, regions of the backscattered energies corresponding to the matrix elements (C, N and O) and Cu were selected. Whereas for STIM, slices of the energy loss spectrum were selected. A dynamic colour scale was used to identify gradient amounts.

The data acquisition, including imaging processing, spectral analysis and quantitative elemental analysis was performed using OMDAQ2007 software (Oxford Microbeams Ltd,

UK) [71]. Elemental concentrations were expressed in μg/g dry weight.

The tested complexes present different states of oxidation for copper (+1 for complex 1 and +2 for complex 2) and different ligand types (monocamphor ^2A for complex 1 and bicamphor ^1B for complex 2). Therefore, these properties may influence the cellular uptake of Cu by OVCAR3 cells and the cellular homeostasis of endogenous elements.

4.2.3 Macro-PIXE

For the analysis of bulk elemental concentrations in samples, macro-PIXE was performed in a dedicated beam line of the IST/CTN Van De Graaff accelerator, using a beam with approximately 0.4 cm^2 area. The samples are analyzed in vacuum. The analyzed samples correspond to acid digested cell extracts. The delivered output is quantitative, giving a precise determination of elemental concentrations in cell extracts. Therefore, the cellular Cu uptake can be confirmed and changes in physiological elements can be also interpreted.

OVCAR3 cells were incubated for 24 hours with the equivalent IC_{50} concentration (72μM) of complex 1, representative of the copper complexes behaviour and selected in order to corroborate the achieved findings with the procedures performed in the nuclear microprobe. Once again, OVCAR3 cells with no treatment were used as control and the uptake of complexes 7 and 9 was also assessed to verify the differences caused by metal core alterations in the drugs. Due to their high cytotoxicity, the treatment time with 7 and 9 complexes was limited to 3 hours (and the concentrations were adjusted to the values of 22μM and 37 μM, respectively) to make sure the cells were not totally destroyed.

After the treatment, the cells were washed with PBS in order to remove the culture medium remains, centrifuged (1300 g, 10 min), freeze-dried and digested using suprapure nitric acid and yttrium (Y) (100 mg/l) as an internal standard. The digestion procedure consisted of ultrasound cycles of 30 min at 60°C and microwave-assisted acid digestion (350 W, 15 s). A 10 μl aliquot of the obtained digested solution was pipetted onto a polycarbonate foil 1.5 μm thick and analysed in the PIXE chamber. The PIXE spectrum analysis was carried out with AXIL software whereas concentration calculation were performed with DATTPIXE computer package [72]. The elemental concentrations of Cu and other endogenous elements were obtained in μg/g dry weight (dw) and converted to μg/g wet weight (ww) as appropriate.

With this assay, the goal was to compare the cellular uptake of the complexes with different metal cores, with the same ligand (monocamphor ^2A) and hence, the influence of the metal properties in the complex behavior towards the treated cells. Therefore, results would help in the comprehension of previous results from the biological assays.

5

Results

5.1 Biological Assays

5.1.1 Cytotoxic Activity

The IC_{50} values obtained in the MTT assay for the complexes are presented in table 5.1. The cytotoxicity values against the non-malignant cell lines (normal fibroblasts, HDF and V79) were used to calculate the selectivity index (SI value), a parameter used to express a compound's *in vitro* efficacy. As can be observed from table 5.1, the IC_{50} values obtained for the two healthy cell lines differ, in particular for copper complex 1 and silver complexes 6 and 7. Therefore, the HDF human cell line, was selected for the calculation of the SI values. The selectivity index is obtained by the quotient $IC_{50}(HDF)/IC_{50}(OVCAR3)$. A SI value < 2 indicates general toxicity of the compound, while a SI value ≥ 10 indicates that the compound has potential to be further investigated as a therapeutic drug [73]. Based on these assumptions, comparing the IC_{50} values obtained for OVCAR3 to those obtained for HDF, it was possible to observe that the majority of compounds have Selectivity Index (SI) values higher than 2 and the copper complexes are the less selective ones. The silver complexes are the more selective, in particular complex 5, that exhibits a high degree of cytotoxic selectivity (SI$>$ 50).

An overall observation led to the conclusion that the copper complexes exhibit lower anticancer activity than the silver and gold complexes no matter the oxidation state of the copper site Cu(I) (1,3) or Cu(II) (2,4) or the mono (1,2,4), or bi-camphor (3) character of the camphorimine ligands. Apparently, the Cu(II) complexes (2,4) display lower cytotoxicity than Cu(I) complexes (1,3) towards normal cells (V79 and HDF).

The gold complexes (8,9) display IC_{50} values lower than the copper complexes by ca. two orders of magnitude either for cancer cells (A2780 and OVCAR3) or normal cells (HDF and V79 fibroblasts), with a slightly higher selectivity (SI) in agreement with a better anticancer performance than the copper complexes. From the camphorimine complexes (Cu, Ag, Au) under study, the silver compounds display the most promising results in what concerns biomedical applications, although their IC_{50} values towards cancer cells are higher than those found for the gold complexes. Nevertheless, their very

low toxicity to normal cells is revealing by a high selectivity (SI) for A2780 and OVCAR3 cells.

The camphorimine ligands by themselves display no cytotoxic activity as later assessed under similar experimental conditions (> 100 μM). The IC_{50} values for Cisplatin were also later obtained for the OVCAR3 and HDF cells for comparison purposes. The obtained values correspond to 1.65 ± 0.57 μM for OVCAR3 cells and 73.6 ± 12 μM for HDF, reaching a SI value of *ca.* 45. All the compounds are more active towards OVCAR3 cells than Cisplatin but they are also more active towards healthy HDF cells with the exception of complexes 5 and 6 that overcome the SI value of reference obtained for the platinum compound.

For comparative purposes, the cytotoxicity of the metal precursors CuCl and $CuCl_2$, $AgNO_3$ and $Ag(CH_3COO)_2$ and $KAu(CN)_2$ was also evaluated (table 5.2) against OVCAR3 cells. With exception of the complexes 4 (Cu(II)) and 7 (Ag(I)) all the other complexes have lower IC_{50} values than their corresponding metal precursors. The silver and gold salts are very active enhancing the activity of the camphorimine derived complexes.

The IC_{50} values measured for each complex demonstrate that they exhibit similar cytotoxicity towards the two ovarian cancer cell lines, thus the subsequent studies were performed with the OVCAR3 cells.

Table 5.1: IC_{50} values at 24h incubation obtained for the camphorimine (copper, silver and gold) complexes by the MTT method. The IC50 values are presented in μM. The selectivity index is obtained by $IC_{50}(HDF)/IC_{50}(OVCAR3)$. The >100 values mean that at 100 µM the cellular viability (% control) is superior than 80% and cannot be determined with the GraphPad prism software.

Complex Reference	A2780	OVCAR3	V79	HDF	SI
1	45.6 ± 11.0	72.4 ± 9.1	34.5 ± 9.7	116 ± 27	1.6
2	49.5 ± 14.0	37.6 ± 8.5	>100	>100	>3
3	43.1 ± 9.1	37.5 ± 7.7	44.9 ± 10.0	48.3 ± 27.0	1.3
4	>100	115 ± 25	>100	>100	>1
5	3.53 ± 0.90	2.24 ± 0.48	>100	>100	>50
6	0.66 ± 0.28	0.63 ± 0.23	3.01 ± 0.90	30.6 ± 8.5	49
7	10.4 ± 2.9	8.99 ± 3.30	34.1 ± 15	276 ± 97	31
8	0.08 ± 0.01	0.08 ± 0.03	0.48 ± 0.06	0.46 ± 0.17	5.7
9	0.04 ± 0.02	0.07 ± 0.01	0.48 ± 0.30	0.59 ± 0.11	8.4

Table 5.2: IC50 values at 24h incubation obtained for the copper, silver and gold precursors by the MTT method. The values are presented in μM.

Precursor	OVCAR3
CuCl	>100
$CuCl_2$	>100
$Ag(NO_3)$	2.66 ± 1.00
$Ag(CH_3COO)$	3.38 ± 2.00
$KAu(CN)_2$	0.49 ± 0.02

5.1.2 Complexes Stability in Solution

The absorption spectra obtained for each complex that allow a qualitative analysis of the complex stability in physiological solution are presented in this section. As described before, four solutions containing the respective complex were evaluated for 48 hours: dissolved in a) 100% DMSO, in b) colorless DMEM with 1% DMSO and in c) colorless DMEM with 1% DMSO and 10% FBS.

Overall, all the complexes are considerably stable when dissolved in DMSO but there is a common disappearance of the initial absorption band between 200 and 300 nm of the spectrum with the addition of DMEM and FBS.

It is possible to distinguish an unstable behavior in Cu complexes (figure 5.1).

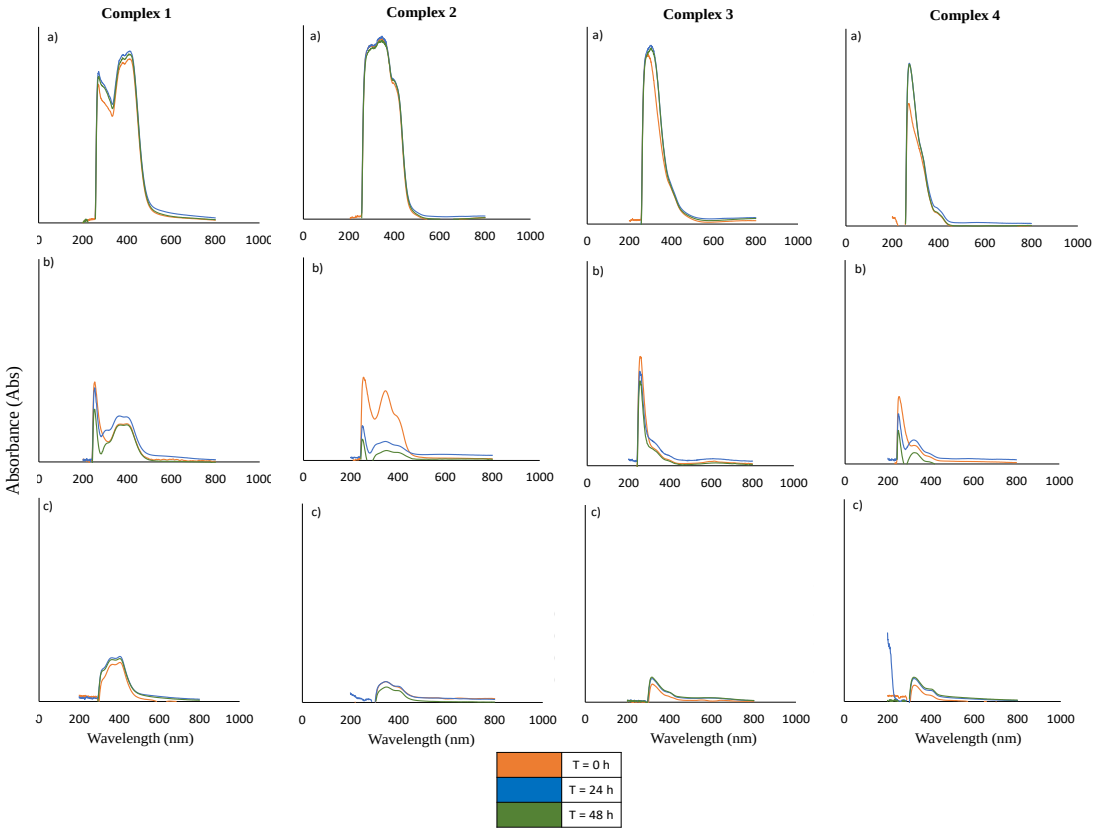

Figure 5.1: UV-Vis spectra of copper complexes (1, 2, 3 and 4) for 0h, 24h and 48 h in DMSO solution (a), in phenol red-free DMEM in the absence (b) and presence of FBS (c).

Especially when the DMEM medium is added, some variations on the absorbance peaks are noticeable over time, as the ones visible for complex 2 solution b) where the absorbance curve for T = 0 h is completely separate and distinct from T = 24 h and T = 48 h. The complex 3 is the one with the most stable behavior among the tested copper compounds for the almost perfect overlapping of the absorption curves for the three solutions a), b) and c) that demonstrates constant absorbance values for the 48 hours of the study

and hence, the preservation of the structure and chemical composition. The complex 1 presented significant instability in DMEM, but not in DMEM supplemented with FBS. This observation represented an interesting finding since the complexes' solutions for the biological studies were prepared in DMEM + 10% FBS.

The Ag(I) (figure 5.2) and Au(I) (figure 5.3) complexes seemed to be more stable confirmed by the maintenance of their absorption bands between 300 and 400 nm (in the three different compositions and with the temporal evolution). Complexes maintain its original form in solution, even after 48h incubation time.

As low concentrations are used in the biological studies, one can expect that both the stability and the solubility are not impaired.

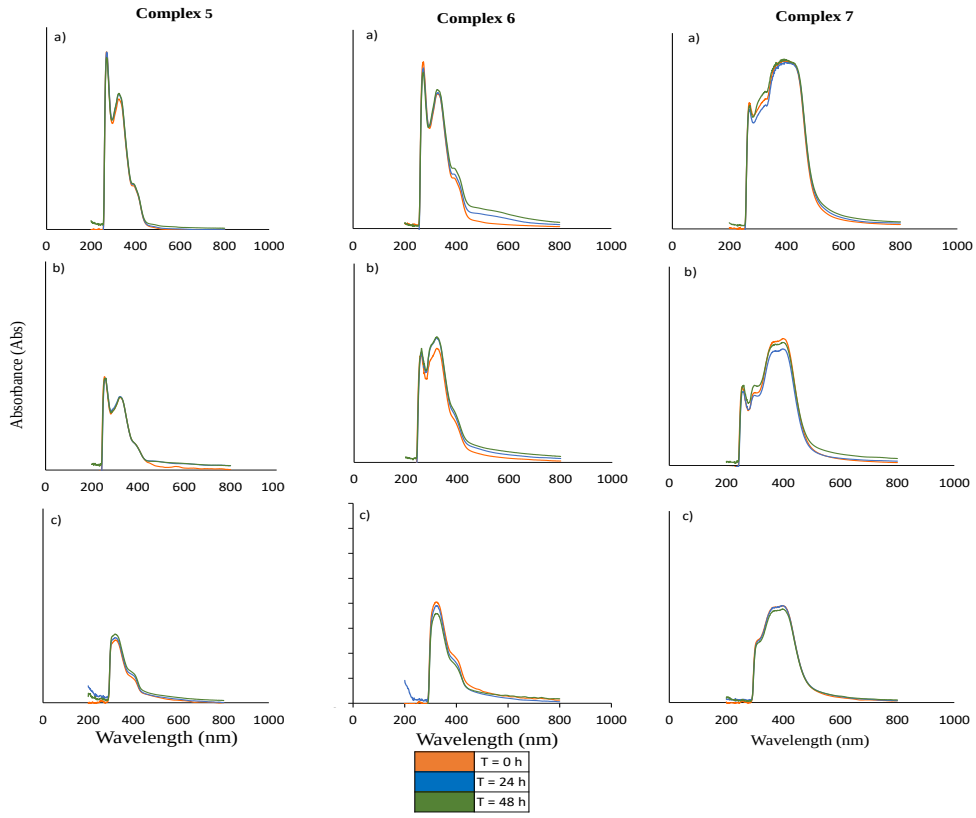

Figure 5.2: UV-Vis spectra of silver complexes (5, 6 and 7) for 0h, 24h and 48 h in DMSO solution (a), in phenol red-free DMEM in the absence (b) and presence of FBS (c).

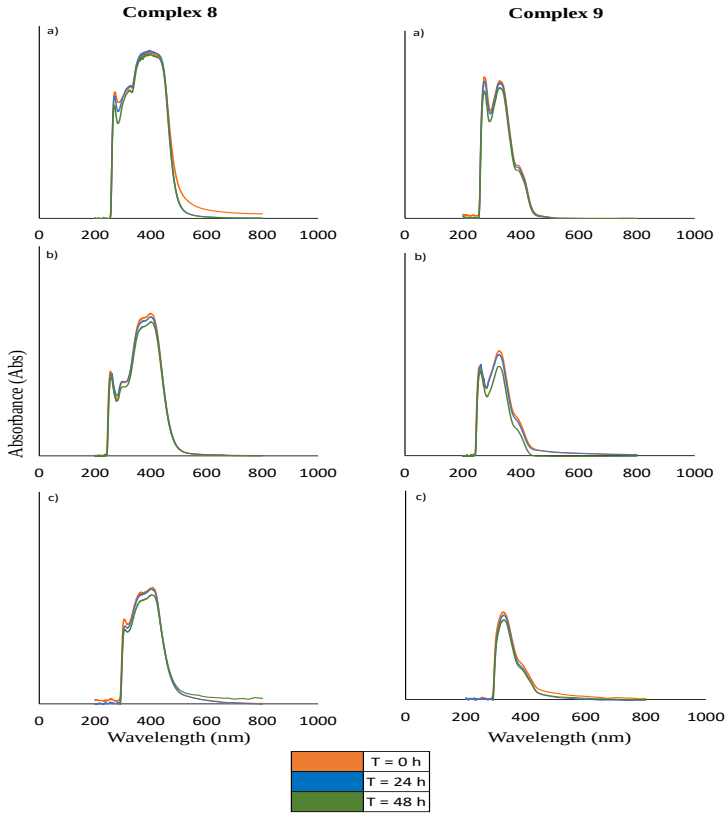

Figure 5.3: UV-Vis spectra of gold complexes (8 and 9) for 0h, 24h and 48 h in DMSO solution (a), in phenol red-free DMEM in the absence (b) and presence of FBS (c).

5.1.3 Complexes-DNA interaction

Considering that the results obtained so far had demonstrated that the copper complexes were less cytotoxic and less stable in culture medium, the studies proceeded by focusing mainly on the silver (5 and 7) and gold complexes (8 and 9) having the monocamphor ligands ${}^{1}A$ and ${}^{2}A$, respectively, while also including complexes 1 and 4 for comparison purposes. As shown in figures 5.4 (copper complexes), 5.5 (silver complexes) and 5.6 (gold complexes), none of the complexes led to changes in the electrophoretic mobility of ϕX174 DNA and consequently, it is possible to conclude that none of them interacts significantly with the DNA molecule. Therefore, their cytotoxicity is mediated by a mechanism of action distinct from that of Cisplatin, which has previously been shown to bind to DNA and induce extensive electrophoretic changes in the DNA's mobility (figure 4.3).

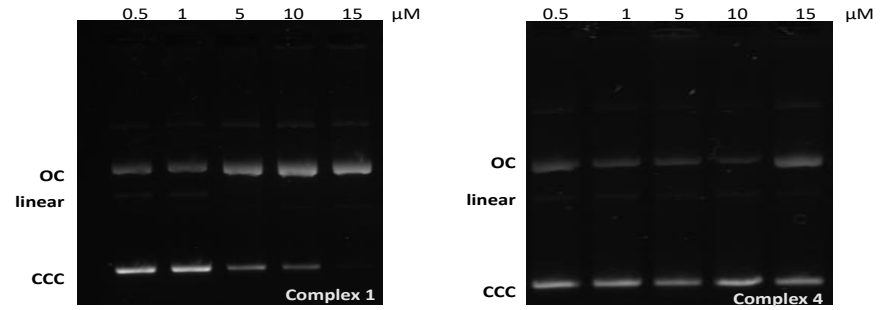

Figure 5.4: Agarose gel electrophoresis of supercoiled ϕX174 DNA incubated with copper complexes 1 and 4, with concentrations of 0.5, 1, 5, 10 and 15 µM. OC, linear and CCC forms of supercoiled DNA are identified.

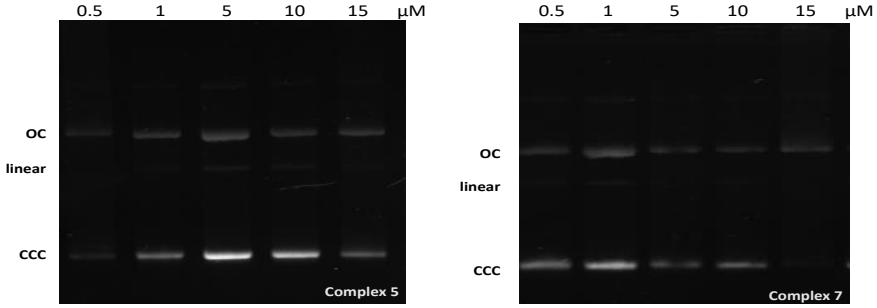

Figure 5.5: Agarose gel electrophoresis of supercoiled ϕX174 DNA incubated with silver complexes 5 and 7, with concentrations of 0.5, 1, 5, 10 and 15 µM. OC, linear and CCC forms of supercoiled DNA are identified.

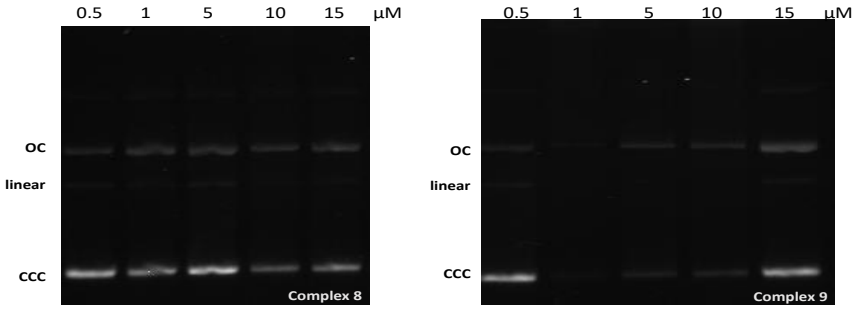

Figure 5.6: Agarose gel electrophoresis of supercoiled ϕX174 DNA incubated with gold complexes 8 and 9, with concentrations of 0.5, 1, 5, 10 and 15 µM. OC, linear and CCC forms of supercoiled DNA are identified.

5.1.4 ROS Production

As depicted on figures 5.7 (copper complexes) and 5.8 (silver and gold complexes), all the complexes induce production of ROS (relative to untreated cells) in OVCAR3 cells. The major evidence of a dose-response effect was observed for copper complex 1 and in general for all other silver and gold complexes. Regarding the influence of the type of

ligands on the induction of ROS, in particular, for the copper complexes, the bicamphor analogs ^1B and ^2B did not induce any significant ROS levels elevation compared with the monocamphor ^1A and ^2A ligands.

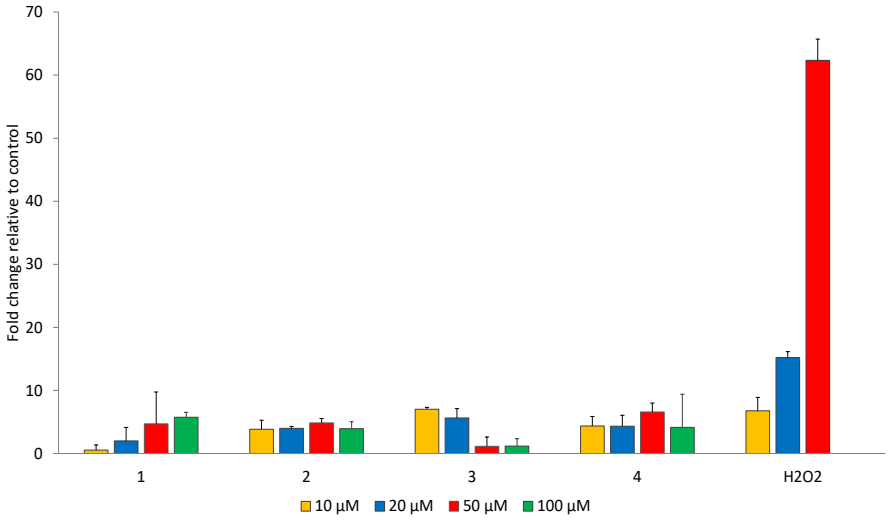

Figure 5.7: Production of ROS, mainly H_2O_2, in OVCAR3 cells treated with complexes 1, 2, 3, 4 at 10, 20, 50 and 100 μM. Results obtained by the H_2DCF−DA method based on the detection of DCF fluorescence. For comparative proposes, H_2O_2 was included in each assay as a positive control. Results of fluorescence intensity are presented as fold change relative to control (untreated OVCAR3 cells) and as mean values ± SD.

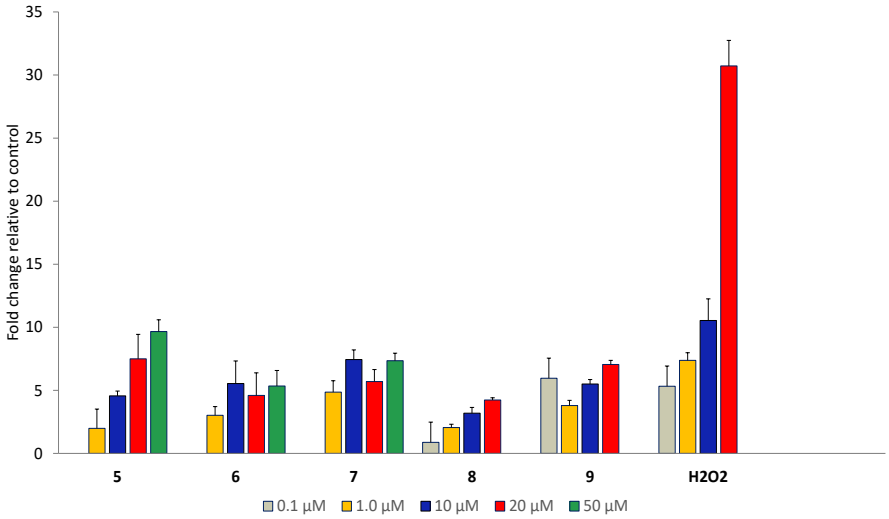

Figure 5.8: Production of ROS, mainly H_2O_2, in OVCAR3 cells treated with 5, 6, 7, 8, 9 at 0.1, 1.0, 10, 20 and 50 μM. Results obtained by the H_2DCFDA method based on the detection of DCF fluorescence. For comparative proposes,H_2O_2 was included in each assay as a positive control. Results of fluorescence intensity are presented as fold change relative to control (untreated OVCAR3 cells) and as mean values ± SD.

The metal precursors were also tested to evaluate their contribution on the production of ROS. The results presented in appendix A demonstrate that the fold change relative to control displayed by the compounds were very low, not exceeding the value (of fold change relative to control) of 1.6, and this result was found only for $CuCl_2$ at a high concentration (100 μM).

The production of superoxide ($O_2^{\bullet -}$) detected with NBT assay is shown in figure 5.9. Considering the superoxide levels elevation above the 100% line in relation to control (being the 100% the superoxide level in the control samples) and the error bar associated to this values, one might conclude that the most significant values results were obtained for complexes 1, 5, 6, 7, 8 and 9. In OVCAR3 cells treated with these complexes, the increase in the superoxide levels is appreciable, especially at higher concentrations. Considering that for this assay only two concentrations were tested, it is not possible to analyse dose-dependent behaviors. Nevertheless, complexes 1, 5, 8 and 9 (not clear for 8) seemed to demonstrate dose-dependent patterns. It is noteworthy that complex 9 induces a considerably higher superoxide production (150 ± 10%) when compared with control at 20 μM.

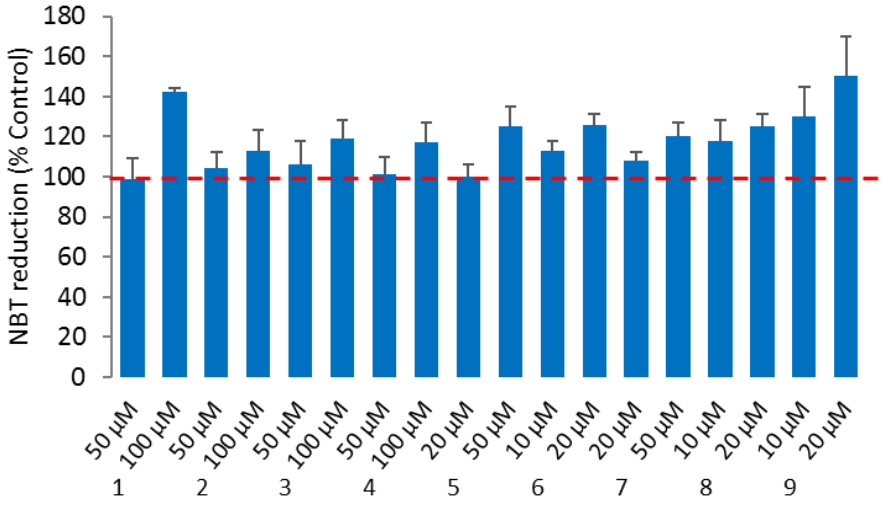

Figure 5.9: Production of superoxide (relative to untreated cells) assessed by the NBT assay in OVCAR3 cells treated with the complexes 1 to 9.

5.1.5 Membrane Lipid Peroxidation

The MDA content for untreated OVCAR3 cells is 0.08 ± 0.02 nmoles/10^6 cells. So, when compared for the values presented for the treated cells it became possible to affirm that a low but important elevation of the basal levels of lipid peroxides was caused by the effect of the complexes 1, 5, 8 and 9 in the cells. Additionally, the MDA levels induced by the complexes correlate with the levels of ROS, pointing to the mechanism of action being involved in the production of ROS and consequently the peroxidation of the membrane

lipids. This is supported by the correlation that seems to exist between the production of ROS and the levels of lipid peroxides particularly for 5, 8 and 9. Noteworthy is the fact that the more selective complexes (5, 9) among the four tested complexes display the highest MDA values.

Table 5.3: Lipid peroxides (MDA) content in the OVCAR3 cells treated for 6 h with 1, 5, 8 and 9 at 100, 50 and 20 μM, respectively. Results are mean ± SD.

Complexes	**MDA (nmoles/10^6 cells)**
1	0.290 ± 0.011
5	1.74 ± 0.27
8	1.09 ± 0.20
9	1.37 ± 0.21

5.2 Cellular Uptake

5.2.1 Macro - PIXE

All the elemental concentrations detected by macro-PIXE performed in OVCAR3 cells treated with the complexes 1, 7 and 9 are listed in table 5.4. The PIXE analysis enabled to detect quantitatively the concentrations of endogenous elements, I.e., K, Ca, Fe, Cu and Zn and evaluating the uptake of Cu, Ag and Au in treated cells, in relation to control samples.

Based on the detected elemental concentrations, the z-score statistical parameter was calculated for each element and sample (table 5.5), except for Au and Ag for their concentration in control samples is null. The z-score values were obtained by subtracting the control mean concentration to the elemental concentration in the sample and dividing the result by the standard deviation associated to control values. This provides information on the number of standard deviations of the elemental concentration in relation to control, in each sample. If z-score is positive or negative, the elemental concentration is above or bellow the mean value of the control sample, respectively. On the other hand, if is approximately zero, no relevant alteration was detected. The z-score value represents a significant alteration when its absolute value is superior to 3, representing an abrupt deviation from the mean value of control.

Table 5.4: Potassium (K), calcium (Ca), iron (Fe), copper (Cu), zinc (Z), silver (Ag) and gold (Au) levels in mg/kg ww obtained by PIXE in OVCAR3 cell pellets untreated (control) and treated with IC_{50} equivalent concentrations of complexes 1, 7 and 9.

	Concentration ± SD (mg/kg ww)						
Sample	**K**	**Ca**	**Fe**	**Cu**	**Zn**	**Ag**	**Au**
Complex 1 (72 μM)	536.7 ± 1.1	49.6 ± 9.3	13.2 ± 0.4	3.4 ± 0.3	10.9 ± 1.7		
Complex 7 (87 μM)	835.7 ± 6.4	17.7 ± 3.3	7.2 ±0.2	0.3 ± 0.005	7.4 ±1.1	19.9 ± 5.6	
Complex 9 (22 μM)	902.3 ± 3.9	49.9 ± 12.6	8.6 ± 0.2	0.9 ± 0.1	6.9 ± 1.3		52.9 ± 1.8
Control	544.1 ± 8.7	42.4 ± 2.4	18.4 ± 0.1	0.7 ± 0.2	8.2 ± 1.2		

Table 5.5: Z-score values for the potassium (K), calcium (Ca), iron (Fe), copper (Cu), zinc (Z), silver (Ag) and gold (Au) concentrations detected in OVCAR3 cells treated with complex 1, 7 and 9.

	Z-score				
Sample	**K**	**Ca**	**Fe**	**Cu**	**Zn**
Complex 1 (72 μM)	-0.8	2.9	-38.4	12.6	2.2
Complex 7 (87 μM)	33.5	-10.1	-82.4	-2.2	-0.7
Complex 9 (22 μM)	41.1	3.1	-72.1	0.8	-1.1

A significant cellular uptake of Cu, Au and Ag, which are the metals associated to the direct structure of the treatment drugs, was clearly observed. Being Cu an endogenous element, it is already present in the control samples but in a trace amount. Therefore the Cu increment in cells treated with complex 1 is meaningful as the concentration in treated cells are 12 standard deviations (SD) above the average Cu concentration in controls. Concerning Au and Ag, which are virtually non-existing in control OVCAR3 cells, the cellular uptake revealed that complex 9 containing Au was more efficiently uptaken by cells than the analogue complex with Ag. The ratio of the concentrations of complexes 9 and 7 in cells is of 2.6 that corresponds to an increase of approximately 35% relative to the ratio of the incubating concentrations.

When control cells were compared to treated ones, relevant alterations were detected for the concentrations of K, Ca and Fe, which are physiological elements. An increase of K concentrations was observed in cells treated with the Ag (7) and Au (9) complexes, whereas in cells treated with the copper complex 1 the K concentrations were unchanged. These changes may reflect the toxicity of complexes 7 and 9 relative to the Cu analogue. Also, a decrease of Ca in cells treated with complex 7 was observed and a major depletion in the Fe levels was detected for the OVCAR3 cells samples treated with the three complexes.

5.2.2 Microprobe

The elemental and density distributions of the OVCAR3 cells treated with the complexes 1 and 2 are represented in figures 5.10 and 5.11, respectively. The control images (untreated OVCAR3 cells) can be found in figure 5.12, and serve as terms of comparison. Establishing a correlative imaging approach with STIM and PIXE maps, the cell morphology can be associated to elemental distributions.

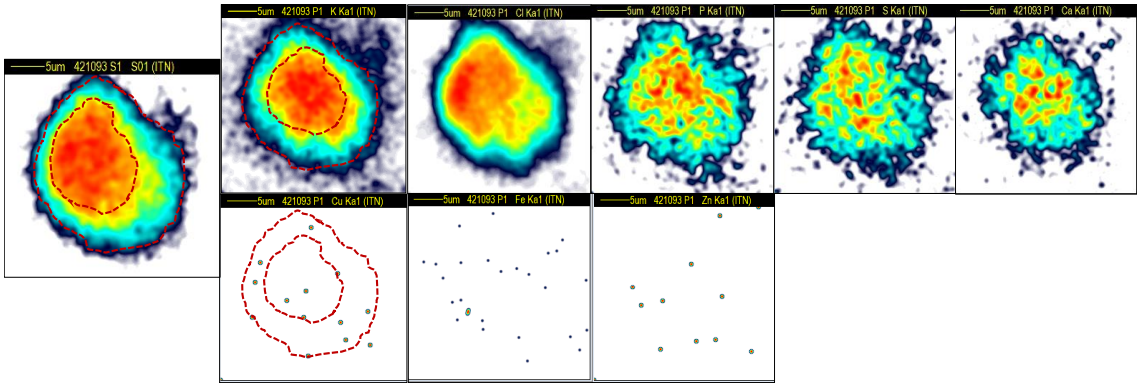

Figure 5.10: Nuclear microscopy images of mass density (STIM) and elemental distribution maps of , K, Ca, P, S, Cu, Fe, and Zn (PIXE) in a single OVCAR3 cell treated with complex 1. The dotted lines in mass and K and Cu maps indicate the cell contour and the nuclear region. The mass density and elemental distribution are represented by a colour gradient with a dynamic scale: high level-red; low level-deep blue.

All the density images for the three cases in study, demonstrate the expected shape of an OVCAR3 cell: ovoid and with a denser central core. This is confirmed by the distribution of the bulk elements - the cellular membrane limits are visible and nucleus indicated for the higher accumulation of this elements for the more intense metabolic activity associated to the nuclear zone. The cells had very low concentrations of trace elements Cu, Fe, and Zn, as evidenced by the low statistics of the maps. The copper distribution maps that would be indicative of the cellular uptake of the complex 1 and 2, the presence of this metal is disperse and residual. Therefore, no conclusions can be drawn from the uptake profile of Cu in OVCAR3 cells treated with both complexes.

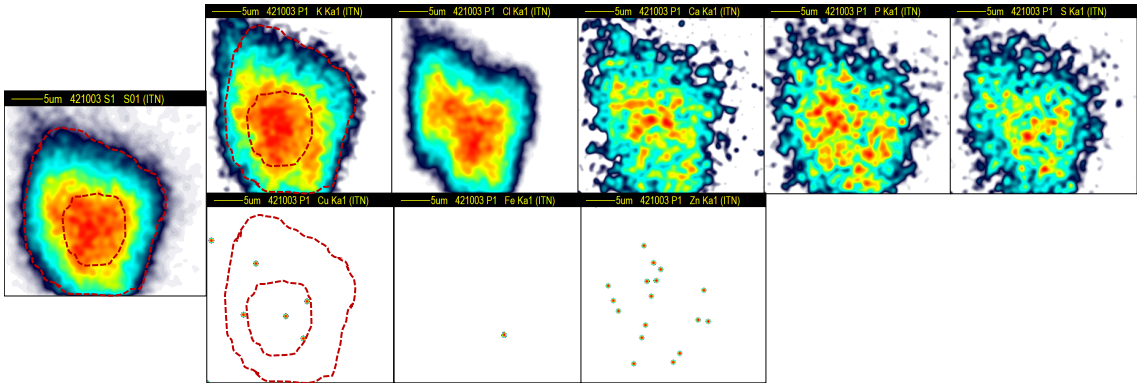

Figure 5.11: Nuclear microscopy images of mass density (STIM) and elemental distribution maps of , K, Ca, P, S, Cu, Fe, and Zn (PIXE) in a single OVCAR3 cell treated with complex 2. The dotted lines in mass and K and Cu maps indicate the cell contour and the nuclear region. The mass density and elemental distribution are represented by a colour gradient with a dynamic scale: high level-red; low level-deep blue.

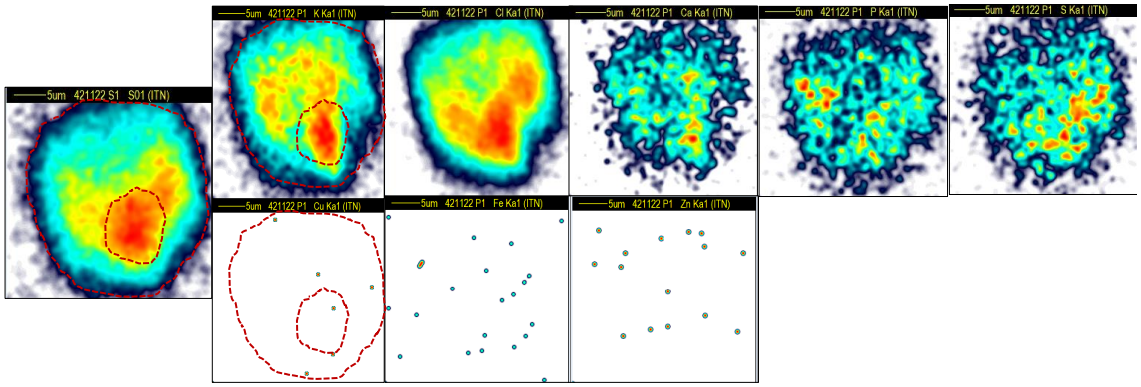

Figure 5.12: Nuclear microscopy images of mass density (STIM) and elemental distribution maps of , K, Ca, P, S, Cu, Fe, and Zn (PIXE) in control (untreated) OVCAR3 cell. The dotted lines in mass and K and Cu maps indicate the cell contour and the nuclear region. The mass density and elemental distribution are represented by a colour gradient with a dynamic scale: high level-red; low level-deep blue.

6

Discussion

Under the scope of medicinal chemistry the development of metal-based complexes have done an important contribute towards the search for novel drugs in order to increase the arsenal of the chemotherapeutics in current use. Platinum (II) drugs like Cisplatin and analogues have been widely used in the clinic to fight against several types of cancers, acting by specifically targeting the DNA.

A great percentage of patients, undergoing chemotherapy, receive a platinum drug either alone or in combination with other chemotherapeutics. Despite their important role in cancer treatment, platinum drugs displayed systemic dose-related toxicity, and frequently drug resistance, which leads to treatment failure. These limitations have strongly motivated the interest in the search for novel metal-based drugs as alternatives to cisplatin. In this direction, several metal complexes other than Pt-based were developed and evaluated as prospective antitumor agents. For a great number of complexes the mechanisms of action often rely on DNA-independent processes such as targeting specific cellular proteins and/or disruption of cellular signaling pathways often accompanied by oxidative stress. ROS (reactive oxygen species) are also signaling molecules and can cause damage to lipids, proteins and DNA.

Cisplatin has been the most used drug for the treatment of ovarian cancer. These types of tumors at a later stage have a very poor prognosis and frequently acquired resistance to cisplatin. In the search for metal-based anticancer agents as alternative to cisplatin, earlier studies by Carvalho et al., using silver complexes with camphor ligands, had showed interesting anticancer activities against both cisplatin sensitive (A2780) and cisplatin resistant (A2780cisR) ovarian cancer cells.

The main goal of the present work was the evaluation of the potential value of selected complexes of Cu(I) (1, 3), Cu(II) (2, 4) Ag(I) (5, 6, 7) and Au(I) (8, 9) containing camphor derivatives (camphorimines) for ovarian cancer treatment.

Results demonstrate a different cytotoxic profile among the three set of complexes. As the ligands did not induce significant cytotoxicity, it is possible to assume that the differences in cytotoxicity are not directly related to the ligands but related with the metal precursors used, in particular the silver and gold salts. The complexes presented herein

are examples of the importance of the metal site and the type of ligands for exploring metal-based complexes with potential applications as anticancer agents.

The copper complexes when compared to the silver and gold ones present a considerable lower activity with IC_{50} values in the range 40 to 70 μM for both ovarian cancer cells. This observation could be the result of their poor stability in the cell media and their low cellular uptake as confirmed by UV-vis spectra and PIXE, respectively. Concerning the influence of the oxidation state of copper, no appreciable differences in activity were observed for Cu(I) and Cu(II) complexes with the monocamphor (^1A, ^2A) and bicamphor (^1B, ^2B) ligands (complexes 1-3). In addition, the lower activity of these copper complexes is consistent with unchanged concentrations of cellular endogenous elements, such as K, Ca and Zn, both in individual cells and in cell pellets. In spite of that, a significant depletion of the iron levels in OVCAR3 cells treated with the IC_{50} equivalent concentration of complex 1 was detected by PIXE. The same happened for cells treated with complexes 7 and 9 (Au and Ag, respectively) but in a more accentuated way. This might be directly associated to the elevation of ROS levels and consequent oxidative stress caused by these complexes. The action of stress proteins (small heat shock proteins, sHsps) correlates with a drastic decrease in the intracellular iron, a catalyser of hydroxyl radical ($OH^{\bullet}$) generation, in order to protect the cells against the oxidative stress [74]. In a similar way to copper, the gold complexes showed no appreciable differences in activity whether the complexation was with the monocamphor ^1A or ^2A ligands (8, 9). The high cytotoxic activity was attributed mainly to their precursor salt. However, the cellular uptake of gold was significant which confirm the better stability of the complexes in the cell media.

The silver complexes showed a different pattern of activity since two salt precursors were used to prepare the respective complexes. The silver acetate was slightly less cytotoxic than the silver nitrate and their respective complexes followed the same trend (7 vs. 5).

Complex 6 displayed considerable activity which could be explained by the two coordinated silver atoms in the molecule. Although, the silver concentration in incubation media was higher than that used for gold complex (37 vs. 22 μM) (7 and 8), the cellular uptake of silver was below the minimum detectable level of PIXE. This correspond to a 2-fold decrease in the uptake of silver relative to gold, in absolute concentration values.

Although, the activity of the silver and gold complexes was relevant the homeostasis in OVCAR3 cells seemed to be relatively preserved. The concentrations of most physiological elements were unchanged, except for iron and potassium for complexes 7 and 9. This alteration in potassium concentrations may be a consequence of increased lipoperoxidation and membrane permeability alteration caused by ROS.

The mechanisms of action of these complexes cannot be attributed to the interaction with the DNA as was observed by electrophoresis, using a single-stranded DNA. None of the complexes led to changes in the electrophoretic mobility of ϕX174 DNA and consequently, it was possible to conclude that none of them interacts significantly with the DNA molecule, in contrast to that was found for Cisplatin.

A great number of anticancer drugs in clinical use act by inducing oxidative stress to cancer cells and consequently cell death. The generation of ROS, mainly peroxides and superoxide, by the copper, silver and gold complexes in the OVCAR3 cells was evaluated using a fluorescent probe and the tetrazolium salt (NBT) for the investigation of the oxidative metabolism in cells. The results obtained showed that the silver and gold complexes induce in a dose-dependent mode generation of ROS. Among the copper complexes, only complex 1 followed a similar trend. ROS can attack membrane lipids to generate lipid peroxides that are further degraded into malondialdehyde (MDA) and 4-hydroxy-2-noneal (4-HNE). This end-products of lipid peroxidation reactions have a cytotoxic role promoting cell death.

The MDA levels induced by complexes were evaluated by the thiobarbituric acid (TBA) assay. After treatment of OVCAR3 cells with complexes 1, 5, 8 and 9 the content of MDA was low but more important than the basal level of lipid peroxides in the untreated OVCAR3 cells. The MDA levels correlate with the levels of ROS, and indicate that the mechanism of action for complexes 1, 5, 8 and 9 could be explained at least in part by the generation of ROS.

Studies are ongoing to explore the mechanism of action in particular for complex 5 that reveal to have a promising biological profile and excellent selectivity being cytotoxic for the ovarian cancer cells while sparing the normal cells.

To sum up, this study intend to give a contribute in the scope of medicinal chemistry to find prospective anticancer drugs with a better profile than Cisplatin and also to have clues on the biological properties of complexes that have in common the same type of ligand but differ in their metal ion.

7

Conclusion

Metal-based drugs is an area with infinite potential and with several peculiarities to discover and comprehend. In the present work, another step was taken and progress was made in the way of unravelling these same capabilities for ovarian cancer treatment by biologically profiling copper, silver, and gold camphorimine complexes.

Complexes of Cu(I) (1, 3), Cu(II) (2, 4) Ag(I) (5, 6, 7) and Au(I) (8, 9) containing camphorimine ligands were selected for their evaluation as potential agents to treat ovarian cancer. The stability of the complexes in cellular media was evaluated by UV-vis spectroscopy, showing changes consistent with instability, i.e., a decrease in intensity of the characteristic peaks of the spectrum, in particular for the copper complexes and in the absence of FBS the bovine serum albumin medium supplement. The silver and gold complexes present higher stability in medium, maintaining its original form in the medium.

The influence of the type of camphorimine ligands on the biological properties of the complexes, in particular for the copper complexes was assessed. The bicamphor analogs ^{1}B and ^{2}B did not induce significant differences compared with the monocamphor ones, and the same finding was true for complexes bearing type ^{1}A (Y= C_6H_5) or type ^{2}A (Y= $C_6H_4NH_2$), the former slightly more lipophilic than the later, 2.94 ± 0.58 vs. 2.25 ± 0.59, respectively.

The cytotoxic activity was evaluated in two human ovarian cancer cell lines: A2780 and OVCAR3, both sensitive to Cisplatin, and the non-tumoral V79 and HDF fibroblasts. In general, all complexes are more cytotoxic towards the ovarian cell lines than the non-tumoral cells, in particular the silver complexes 5 - 7. With exception of copper complexes, the silver and gold camphorimine complexes presented better cytotoxic profile when compared with Cisplatin.

The camphorimine ligands did not induce appreciable cytotoxicity (IC_{50}> 100 μM). However, the metal precursors silver nitrate, silver acetate and particularly potassium dicyanoaurate displayed cytotoxic activities comparable to their corresponding complexes.

Overall, the silver complexes showed higher selectivity towards the ovarian cancer cells as well as higher selectivity indexes. The cytotoxicity data obtained for complexes

1, 5 and 9 seemed to be correlated with their cellular uptake. In fact, the quantification by PIXE of complex 1 in whole OVCAR3 cells indicate only vestigial concentrations of copper inside the cells which is also in agreement with complex´s stability in cellular medium.

The mechanism of cell death by these camphorimine complexes seemed to be related with their ability to induce different types of oxygen radicals (ROS), namely peroxides and lipoperoxides. Studies are ongoing in order to obtain more data related with the mechanism of action for these camphorimine complexes in particular for the best performing complex 5. To better understand the implications of these results, it would be interesting to address some of the limitations of the conducted studies in this dissertation. The alterations on the drug's pharmacokinetics and pharmacodynamics when tested in vivo is a fundamental question and some of the most promising discovered compounds (like complex 5) might suffer great changes when applied to a whole organism, instead of isolated cell lines. Indeed, it is noteworthy that there is a near future prospect of evaluating the effects of the application of complex 5 in zebra fish embryos. It would be also appealing to obtain further images on the cellular distribution of the silver and gold complexes, especially for complex 5, for comparison purposes with the copper complexes'results.

Bibliography

[1] A. Desai et al. "Epithelial ovarian cancer: An overview". In: *World Journal of Translational Medicine* 3.1 (2014), pp. 1–8. DOI: 10.5528/wjtm.v3.i1.1.

[2] J. M. Cardoso et al. "Synthesis of Ag(I) camphor sulphonylimine complexes and assessment of their cytotoxic properties against cisplatin-resistant A2780cisR and A2780 cell lines". In: *Journal of Inorganic Biochemistry* 166 (2017), pp. 55–63. DOI: 10.1016/j.jinorgbio.2016.11.003.

[3] S. J. Mulware. "The Review of Nuclear Microscopy Techniques : An Approach for Nondestructive Trace Elemental Analysis and Mapping of Biological Materials". In: *Journal of Biophysics* 2015 (2015). DOI: 10.1155/2015/740751Review.

[4] A. A. Bettiol, Z. Mi, and F. Watt. "High-resolution fast ion microscopy of single whole biological cells". In: *Applied Physics Reviews* 3 (2016). DOI: 10.1063/1.4971414.

[5] A. Carmona, G. Devès, and R. Ortega. "Quantitative micro-analysis of metal ions in subcellular compartments of cultured dopaminergic cells by combination of three ion beam techniques". In: *Analytical and Bioanalytical Chemistry* 390.6 (2008), pp. 1585–1594. DOI: 10.1007/s00216-008-1866-6.

[6] T. Pinheiro, M. D. Ynsa, and L. C. Alves. "Imaging biological structures with a proton microprobe". In: *Modern Research and Educational Topics in Microscopy* 3 (2007), pp. 237–244.

[7] S. Johansson et al. *Particle-Induced X-Ray Emission Spectrometry (PIXE)*. Chemical Analysis: A Series of Monographs on Analytical Chemistry and Its Applications. Wiley, 1995. ISBN: 9780471589440. URL: https://books.google.pt/books?id=zKgFMQrfiH8C.

[8] "Depth distribution of particles in plastics in sea-water". PhD thesis. Thesis to obtain the Master of Science Degree in Engineering Physics in University of Lisbon, Instituto Superior Técnico, 2018.

[9] E.-C. Yim, H.-J. Kim, and S.-J. Kim. "Acute toxicity assessment of camphor in biopesticides by using Daphnia magna and Danio rerio". In: *Environmental Health and Toxicology* 29.March 2015 (2014). DOI: 10.5620/eht.2014.29.e2014008.

[10] G. W. Grime. "The "Q factor"method: Quantitative microPIXE analysis using RBS normalisation". In: *Nuclear Instruments and Methods in Physics Research, Section B: Beam Interactions with Materials and Atoms* 109 (1996), pp. 170–174. DOI: 10.1016/0168-583X(95)00901-9.

[11] L. Lemelle et al. "Nano-imaging trace elements at organelle levels in substantia nigra overexpressing α-synuclein to model Parkinson's disease". In: *Communications biology* 3.1 (2020), pp. 1–10.

[12] C. J. Fahrni. "Biological applications of X-ray fluorescence microscopy: exploring the subcellular topography and speciation of transition metals". In: *Current opinion in chemical biology* 11.2 (2007), pp. 121–127.

[13] P. Aguer et al. "Skin morphology and layer identification using different STIM geometries". In: *Nuclear Instruments and Methods in Physics Research, Section B: Beam Interactions with Materials and Atoms* 231.1-4 (2005), pp. 292–299. DOI: 10.1016/j.nimb.2005.01.073.

[14] J. Pallon et al. "An off-axis STIM procedure for precise mass determination and imaging". In: *Nuclear Instruments and Methods in Physics Research, Section B: Beam Interactions with Materials and Atoms*. Vol. 219-220. 1-4. 2004, pp. 988–993. DOI: 10.1016/j.nimb.2004.01.201.

[15] A. Verıssimo et al. "Nuclear microscopy: a tool for imaging elemental distribution and percutaneous absorption in vivo". In: *Microscopy research and technique* 70.4 (2007), pp. 302–309.

[16] S. Ghosh. "Cisplatin: The first metal based anticancer drug". In: *Bio-organic chemistry* 88 (2019).

[17] E. Smolle et al. "Targeting Signaling Pathways in Epithelial Ovarian Cancer". In: *International Journal of Molecular Sciences* 14 (2012), pp. 9536–9555. DOI: 10.3390/ijms14059536.

[18] P. Tudrej et al. "Establishment and characterization of the novel high-grade serous ovarian cancer cell line OVPA8". In: *International Journal of Molecular Sciences* 19.7 (2018), p. 2080. DOI: 10.3390/ijms19072080.

[19] S. Lheureux et al. "Epithelial ovarian cancer". In: *The Lancet* 393.10177 (2019), pp. 1240–1253. DOI: 10.1016/S0140-6736(18)32552-2.

[20] S. L. Coleridge et al. "Neoadjuvant chemotherapy before surgery versus surgery followed by chemotherapy for initial treatment in advanced ovarian epithelial cancer". In: *Cochrane Database of Systematic Reviews* 7 (2021). DOI: 10.1002/14651858.CD005343.pub6.

[21] I. Meinhold-Heerlein and S. Hauptmann. "The heterogeneity of ovarian cancer". In: *Archives of Gynecology and Obstetrics* 289.2 (2014), pp. 237–239. DOI: 10.1007/s00404-013-3114-3.

[22] M. J. Meegan and N. M. O'Boyle. "Special issue "anticancer drugs"". In: *Pharmaceuticals* 12.3 (2019), p. 134.

[23] S. A. Aldossary. "Review on pharmacology of cisplatin: Clinical use, toxicity and mechanism of resistance of cisplatin". In: *Biomedical and Pharmacology Journal* 12.1 (2019), pp. 7–15. DOI: 10.13005/bpj/1608.

[24] K. D. Mjos and C. Orvig. "Metallodrugs in medicinal inorganic chemistry". In: *Chemical Reviews* 114.8 (2014), pp. 4540–4563. DOI: 10.1021/cr400460s.

[25] *Cisplatina*. URL: https://stringfixer.com/pt/Cisplatin (visited on 09/11/2021).

[26] K. J. Davis et al. "Does cytotoxicity of metallointercalators correlate with cellular uptake or DNA affinity?" In: *Dalton Transactions* 41.31 (2012), pp. 9417–9426. DOI: 10.1039/c2dt30217a.

[27] P. Moretto et al. "Nuclear microanalysis of platinum and trace elements in cisplatin-resistant human ovarian adenocarcinoma cells". In: *Nuclear Inst. and Methods in Physics Research, B* 104.1-4 (1995), pp. 292–298. DOI: 10.1016/0168-583X(95)00407-6.

[28] R. Oun, Y. E. Moussa, and N. J. Wheate. "The side effects of platinum-based chemotherapy drugs: A review for chemists". In: *Dalton Transactions* 47.19 (2018), pp. 6645–6653. DOI: 10.1039/c8dt00838h.

[29] U. Ndagi, N. Mhlongo, and M. E. Soliman. "Metal complexes in cancer therapy – An update from drug design perspective". In: *Drug Design, Development and Therapy* 11 (2017), pp. 599–616. DOI: 10.2147/DDDT.S119488.

[30] S. Monro et al. "Transition Metal Complexes and Photodynamic Therapy from a Tumor-Centered Approach: Challenges, Opportunities, and Highlights from the Development of TLD1433". In: *Chemical Reviews* 119.2 (2019), pp. 797–828. DOI: 10.1021/acs.chemrev.8b00211.

[31] M. F. N. Carvalho et al. "Ag(I) camphor complexes: antimicrobial activity by design". In: *Journal of Inorganic Biochemistry* 199.June (2019). DOI: 10.1016/j.jinorgbio.2019.110791.

[32] T. Makovec. "Cisplatin and beyond: Molecular mechanisms of action and drug resistance development in cancer chemotherapy". In: *Radiology and Oncology* 53.2 (2019), pp. 148–158. DOI: 10.2478/raon-2019-0018.

[33] C. Marzano et al. "Copper Complexes as Anticancer Agents". In: *Anti-Cancer Agents in Medicinal Chemistry* 9.2 (2012), pp. 185–211. DOI: 10.2174/187152009787313837.

[34] O. Krasnovskaya et al. "Copper coordination compounds as biologically active agents". In: *International Journal of Molecular Sciences* 21.11 (2020). DOI: 10.3390/ijms21113965.

[35] J. Ceramella et al. "From coins to cancer therapy: Gold, silver and copper complexes targeting human topoisomerases". In: *Bioorganic & Medicinal Chemistry Letters* 30.3 (2020), p. 126905.

[36] D. Denoyer, S. A. S. Clatworthy, and M. A. Cater. "16. COPPER COMPLEXES IN CANCER THERAPY". In: *Metallo-Drugs: Development and Action of Anticancer Agents*. Ed. by A. Sigel et al. De Gruyter, 2018, pp. 469–506. DOI: doi:10.1515/9783110470734-016. URL: https://doi.org/10.1515/9783110470734-016.

[37] P. Nunes et al. "Copper Complexes with 1,10-Phenanthroline Derivatives: Underlying Factors Affecting Their Cytotoxicity". In: *Inorganic Chemistry* 59.13 (2020), pp. 9116–9134. DOI: 10.1021/acs.inorgchem.0c00925.

[38] A. D. Zuberbühler. "Kinetics and thermodynamics of dioxygen interaction with copper". In: *Bioorganic and Medicinal Chemistry Letters* 66.3 (1991), pp. 249–257. ISSN: 01672991. DOI: 10.1016/S0167-2991(08)62840-2.

[39] C. Nardon, G. Boscutti, and D. Fregona. "Beyond platinums: gold complexes as anticancer agents". In: *Anticancer research* 34.1 (2014), pp. 487–492.

[40] S. A. Sousa et al. "On the path to gold: Monoanionic Au bisdithiolate complexes with antimicrobial and antitumor activities". In: *Journal of Inorganic Biochemistry* 202.September 2019 (2020), p. 110904. DOI: 10.1016/j.jinorgbio.2019.110904.

[41] C. I. Yeo, K. K. Ooi, and E. R. Tiekink. "Gold-based medicine: A paradigm shift in anti-cancer therapy?" In: *Molecules* 23.6 (2018), pp. 14–23. DOI: 10.3390/molecules23061410.

[42] T. S. Reddy et al. "Potent and Selective Cytotoxic and Anti-inflammatory Gold(III) Compounds Containing Cyclometalated Phosphine Sulfide Ligands". In: *Chemistry - A European Journal* 25.62 (2019), pp. 14089–14100. ISSN: 15213765. DOI: 10.1002/chem.201903388.

[43] X. Liang et al. "Recent advances in the medical use of silver complex". In: *European Journal of Medicinal Chemistry* 157 (2018), pp. 62–80. DOI: 10.1016/j.ejmech.2018.07.057.

[44] J. P. Costa et al. "Key parameters on the antibacterial activity of silver camphor complexes". In: *Antibiotics* 10.2 (2021), pp. 1–14. DOI: 10.3390/antibiotics10020135.

[45] S. Medici et al. "Medical Uses of Silver: History, Myths, and Scientific Evidence". In: *Journal of Medicinal Chemistry* 62.13 (2019), pp. 5923–5943. DOI: 10.1021/acs.jmedchem.8b01439.

[46] A. Aydin et al. "Anticancer activities and mechanism of action of 2 novel metal complexes, $C_{16}H_{34}N_8O_5Ag_2Cd$ and $C_{11}H_{16}N_7O_2Ag_3Ni$". In: *Turkish Journal of Biology* 38.6 (2014), pp. 948–955. DOI: 10.3906/biy-1405-68.

[47] M. Rendošová et al. "Silver pyridine-2-sulfonate complex - its characterization, DNA binding, topoisomerase I inhibition, antimicrobial and anticancer response". In: *Journal of Inorganic Biochemistry* 186 (2018), pp. 206–216. DOI: 10.1016/j.jinorgbio.2018.06.006.

[48] M. F. N. Carvalho et al. "Search for cytotoxic compounds against ovarian cancer cells: Synthesis, characterization and assessment of the activity of new camphor carboxylate and camphor carboxamide silver complexes". In: *Journal of Inorganic Biochemistry* 188 (2018), pp. 88–95. DOI: 10.1016/j.jinorgbio.2018.08.011.

[49] R. A. Ware et al. "The Therapeutic and medicinal Use of Camphor in Ordinary Life". In: *International Journal of Research in Engineering, Science and Management* 3.5 (2020), pp. 10–11.

[50] T. A. Fernandes et al. "Insight into the cytotoxicity of polynuclear Cu(I) camphor complexes". In: *Polyhedron* 87 (2015), pp. 215–219. DOI: 10.1016/j.poly.2014.11.020.

[51] W. Chen, I. Vermaak, and A. Viljoen. "Camphor-A fumigant during the black death and a coveted fragrant wood in ancient egypt and babylon-A review". In: *Molecules* 18.5 (2013), pp. 5434–5454. DOI: 10.3390/molecules18055434.

[52] J. M. Cardoso et al. "Antibacterial activity of silver camphorimine coordination polymers". In: *Dalton Transactions* 45.16 (2016), pp. 7114–7123. DOI: 10.1039/c6dt00099a.

[53] A. Petrović et al. "Synthesis of Camphor-Derived Bis(pyrazolylpyridine) Rhodium(III) Complexes: Structure-Reactivity Relationships and Biological Activity". In: *Inorganic Chemistry* 58.1 (2019), pp. 307–319. ISSN: 1520510X. DOI: 10.1021/acs.inorgchem.8b02390.

[54] T. E. Kokina et al. "Synthesis, structure, and cytotoxicity of complexes of zinc(II), palladium(II), and copper(I) chlorides with ()-camphor thiosemicarbazone". In: *Polyhedron* 163 (2019), pp. 121–130. DOI: 10.1016/j.poly.2019.02.020. URL: https://doi.org/10.1016/j.poly.2019.02.020.

[55] N. Ribeiro et al. "New Cu(II) complexes with pyrazolyl derived Schiff base ligands: Synthesis and biological evaluation". In: *Journal of Inorganic Biochemistry* 174.May (2017), pp. 63–75. DOI: 10.1016/j.jinorgbio.2017.05.011.

[56] B. Dominelli et al. "Mechanisms underlying the cytotoxic activity of syn/anti-isomers of dinuclear Au(I) NHC complexes". In: *European Journal of Medicinal Chemistry* 203 (2020), pp. 1–11. DOI: 10.1016/j.ejmech.2020.112576.

[57] C. H. G. Jakob et al. *Antiproliferative Activity of Functionalized Histidine-derived Au(I) bis-NHC Complexes for Bioconjugation*. 2020.

[58] C. Sanchez-Cano et al. "Synchrotron X-Ray FluorescenceNanoprobe Reveals Target Sites for Organo-Osmium Complex in HumanOvarian Cancer Cells". In: *Chemistry A European Journal* 23 (2017), pp. 2512–2516. DOI: 10.1002/chem.201605911.

[59] J. L. Wedding et al. "Intracellular distribution and stability of a luminescent rhenium(i) tricarbonyl tetrazolato complex using epifluorescence microscopy in conjunction with X-ray fluorescence imaging". In: *Metallomics* 9.4 (2017), pp. 382–390. DOI: 10.1039/c6mt00243a. URL: http://dx.doi.org/10.1039/C6MT00243A.

[60] E. M. Bolitho et al. "Single-Cell Chemistry of Photoactivatable Platinum Anticancer Complexes". In: *Journal of the American Chemical Society* 143.48 (2021), pp. 20224–20240. DOI: 10.1021/jacs.1c08630.

[61] F. Rivas et al. "Pt-Fe ferrocenyl compounds with hydroxyquinoline ligands show selective cytotoxicity on highly proliferative cells". In: *Journal of Inorganic Biochemistry* 199 (2019). DOI: 10.1016/j.jinorgbio.2019.110779.

[62] C. P. Matos et al. "Exploring the cytotoxic activity of new phenanthroline salicylaldimine Zn(II) complexes". In: *Journal of Inorganic Biochemistry* 198 (2019). DOI: 10.1016/j.jinorgbio.2019.110727.

[63] L. D. S. Yadav. *Organic spectroscopy*. Springer Science & Business Media, 2013.

[64] N. Vamsikrishna et al. "Synthesis, structural characterization, DNA interaction, antibacterial and cytotoxicity studies of bivalent transition metal complexes of 6-aminobenzothiazole Schiff base". In: *Inorganic Chemistry Communications* 113 (2020). DOI: 10.1016/j.inoche.2020.107767.

[65] S. Gama et al. "Synthesis and Biological Studies of Pyrazolyl-Diamine PtII Complexes Containing Polyaromatic DNA-Binding Groups". In: *ChemBioChem* 13.16 (2012), pp. 2352–2362. DOI: 10.1002/cbic.201200472.

[66] Z. Nova et al. "Short-term versus long-term culture of A549 cells for evaluating the effects of lipopolysaccharide on oxidative stress, surfactant proteins and cathelicidin LL-37". In: *International Journal of Molecular Sciences* 21.3 (2020), pp. 1–17. DOI: 10.3390/ijms21031148.

[67] A. V. Snezhkina et al. "ROS generation and antioxidant defense systems in normal and malignant cells". In: *Oxidative Medicine and Cellular Longevity* 2019 (2020). DOI: 10.1155/2019/6175804.

[68] B. Perillo et al. "ROS in cancer therapy: the bright side of the moon". In: *Experimental and Molecular Medicine* 52.2 (2020), pp. 192–203. DOI: 10.1038/s12276-020-0384-2. URL: https://doi.org/10.1038/s12276-020-0384-2.

[69] R&D Systems. *TBARS Parameter™ Kit for Measuring Oxidative Stress*. URL: https://www.rndsystems.com/product-highlights/tbars-parameter-kit-measuring-oxidative-stress (visited on 07/02/2022).

[70] L. C. Alves et al. "Micron-scale analysis of SiC/SiCf composites using the new Lisbon nuclear microprobe". In: *Nuclear Instruments and Methods in Physics Research, Section B: Beam Interactions with Materials and Atoms* 161 (2000), pp. 334–338. DOI: 10.1016/S0168-583X(99)00768-5.

[71] Oxford Microbeams Ltd. *Oxford Microbeams Ltd.* 2019. URL: http://www.microbeams.co.uk/%20http://www.microbeams.co.uk/download.html (visited on 03/29/2022).

[72] M. A. Barreiros et al. "Quality assurance of X-ray spectrometry for chemical analysis". In: *Spectrochimica Acta - Part B Atomic Spectroscopy* 56.11 (2001), pp. 2095–2106. DOI: 10.1016/S0584-8547(01)00285-3.

[73] O. A. Peña-Morán et al. "Cytotoxicity, post-treatment recovery, and selectivity analysis of naturally occurring podophyllotoxins from Bursera fagaroides var. fagaroides on breast cancer cell lines". In: *Molecules* 21.8 (2016). DOI: 10.3390/molecules21081013.

[74] M. A. Liebert et al. "and by Decreasing Iron Intracellular Levels". In: *Methods in Enzymology* 7.75 (2005), pp. 414–424.

A

Metal Precursors ROS Production

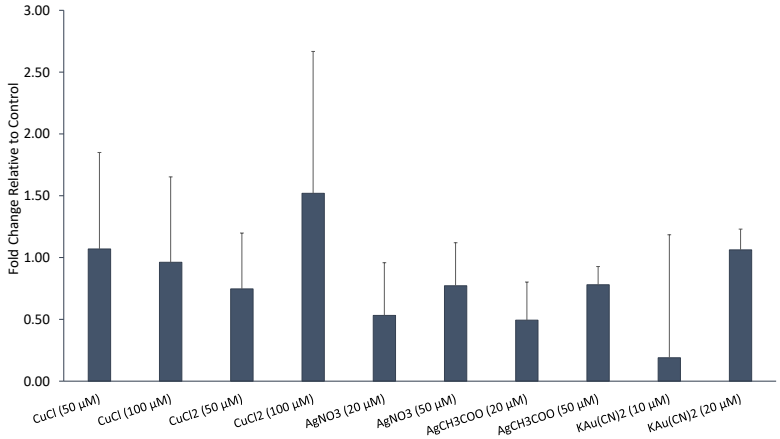

Figure A.1: Production of ROS, mainly H_2O_2, in OVCAR3 cells treated with the metal precursors of the complexes in selected concentrations. Results obtained by the H_2DCFDA method based on the detection of DCF fluorescence and presented in relation to the ones obtained for untreated OVCAR3 cells.

B

MDA Standard Curve

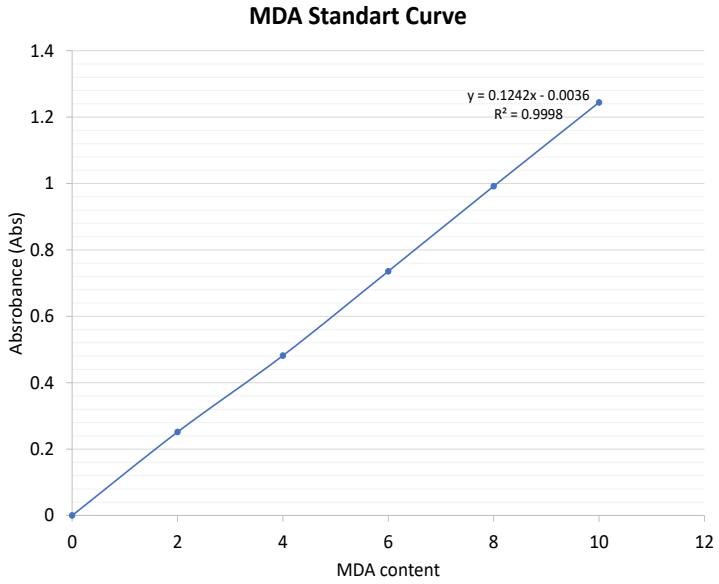

Figure B.1: MDA standart curve, respective equation (y = 0.1242x - 0.0036) and linear regression index (R^2 = 0.9998) obtained quantifying the absorbance of the various MDA standard samples.

C

Dose-Response Curves

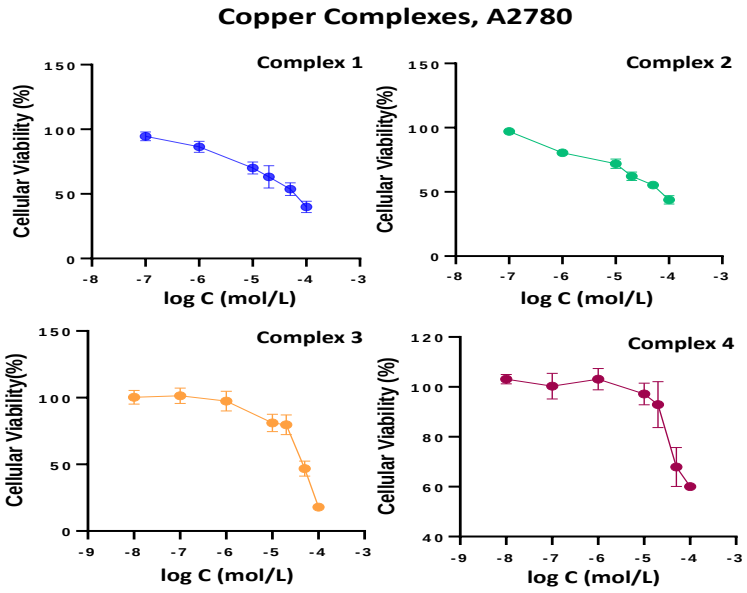

Figure C.1: Dose-response curve obtained with GraphPad Prism software (vs. 5.0) for A2780 cells treated with the copper complexes 1, 2, 3 and 4. The cellular viability *vs.* treatment concentrations is presented.

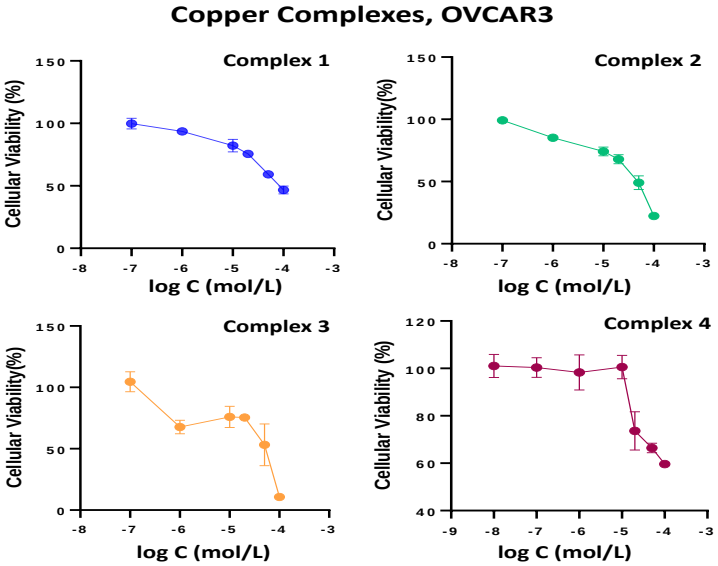

Figure C.2: Dose-response curve obtained with GraphPad Prism software (vs. 5.0) for OVCAR3 cells treated with the copper complexes 1, 2, 3 and 4. The cellular viability *vs.* treatment concentrations is presented.

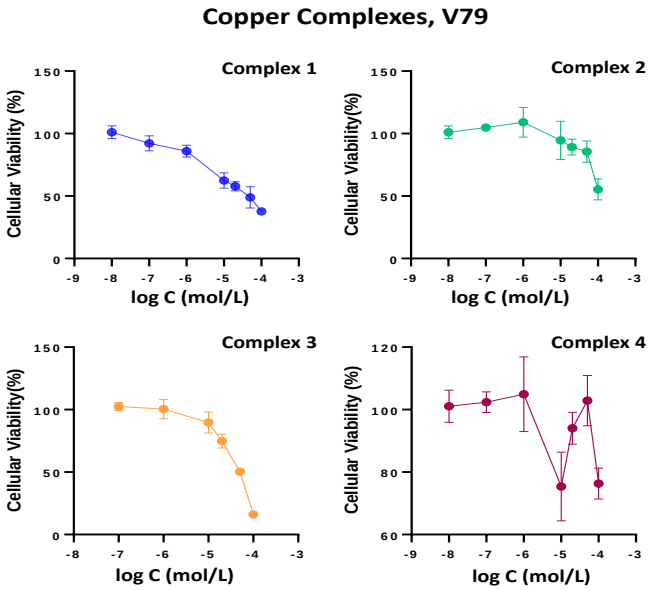

Figure C.3: Dose-response curve obtained with GraphPad Prism software (vs. 5.0) for V79 cells treated with the copper complexes 1, 2, 3 and 4. The cellular viability *vs.* treatment concentrations is presented.

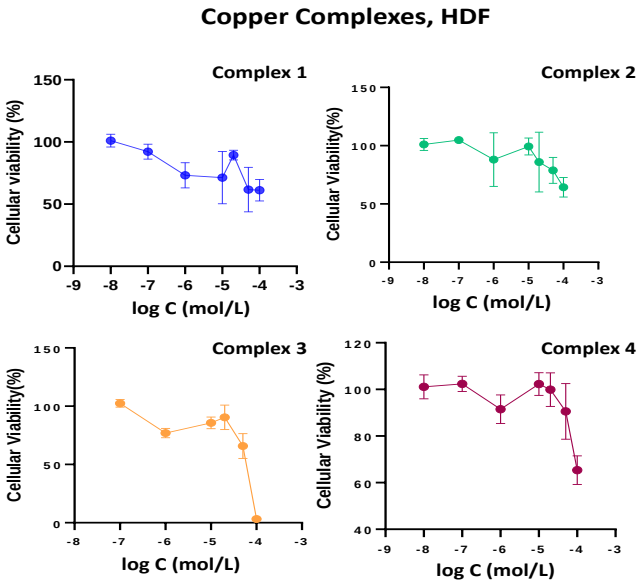

Figure C.4: Dose-response curve obtained with GraphPad Prism software (vs. 5.0) for HDF cells treated with the copper complexes 1, 2, 3 and 4. The cellular viability *vs.* treatment concentrations is presented.

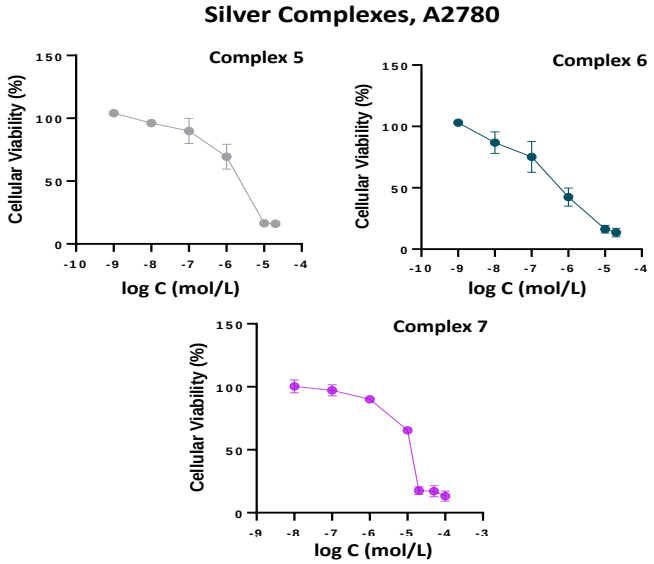

Figure C.5: Dose-response curve obtained with GraphPad Prism software (vs. 5.0) for A2780 cells treated with the copper complexes 5, 6 and 7. The cellular viability *vs.* treatment concentrations is presented.

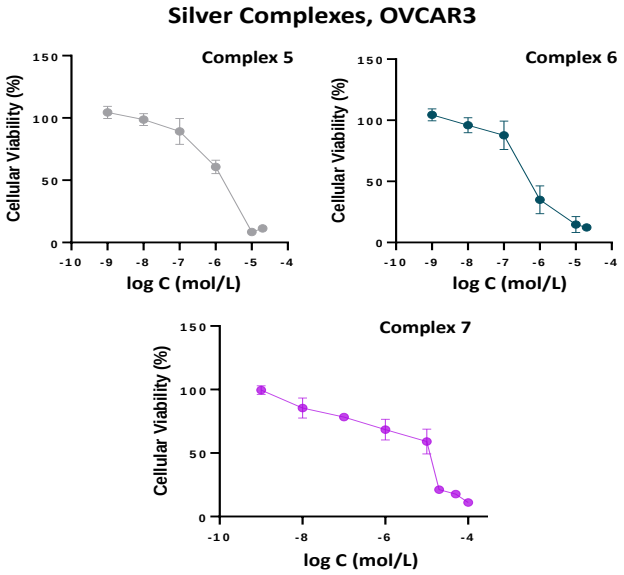

Figure C.6: Dose-response curve obtained with GraphPad Prism software (vs. 5.0) for OVCAR3 cells treated with the copper complexes 5, 6 and 7. The cellular viability *vs.* treatment concentrations is presented.

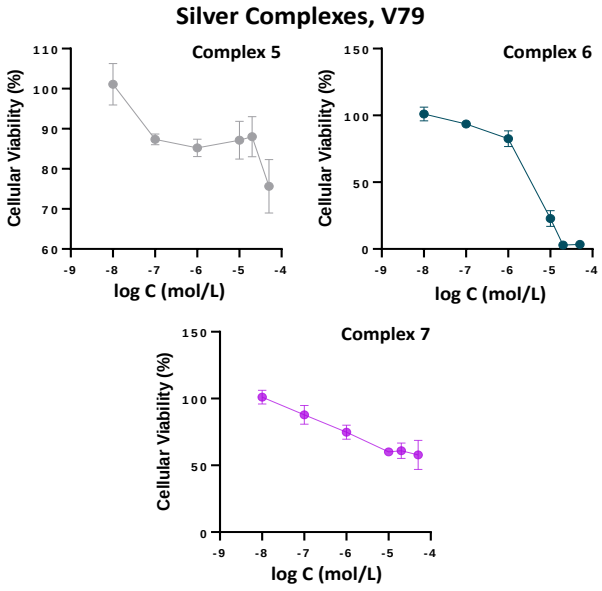

Figure C.7: Dose-response curve obtained with GraphPad Prism software (vs. 5.0) for V79 cells treated with the copper complexes 5, 6 and 7. The cellular viability *vs.* treatment concentrations is presented.

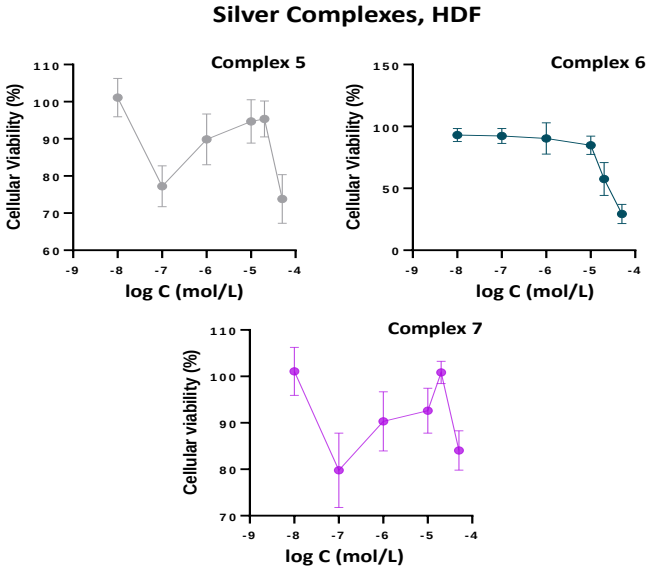

Figure C.8: Dose-response curve obtained with GraphPad Prism software (vs. 5.0) for HDF cells treated with the copper complexes 5, 6 and 7. The cellular viability *vs.* treatment concentrations is presented.

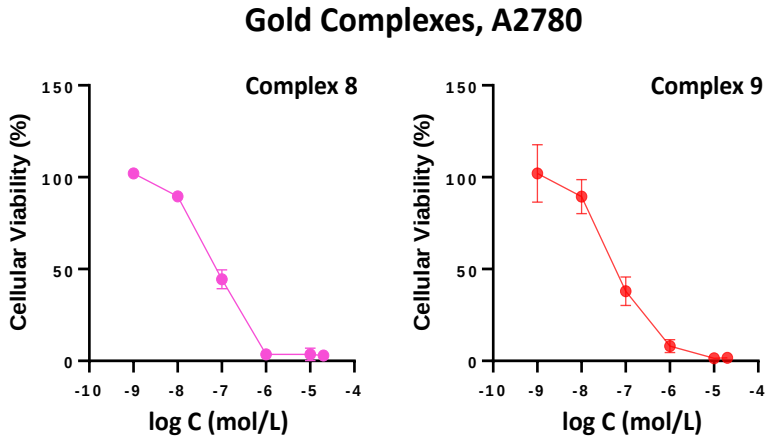

Figure C.9: Dose-response curve obtained with GraphPad Prism software (vs. 5.0) for A2780 cells treated with the copper complexes 8 and 9. The cellular viability *vs.* treatment concentrations is presented.

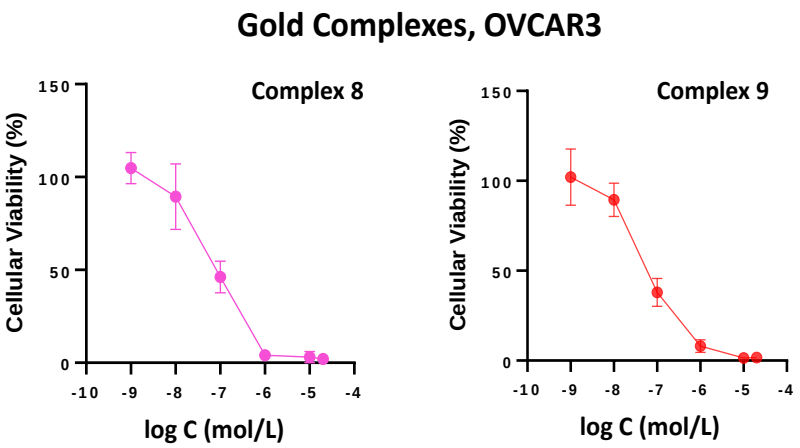

Figure C.10: Dose-response curve obtained with GraphPad Prism software (vs. 5.0) for OVCAR3 cells treated with the copper complexes 8 and 9. The cellular viability *vs.* treatment concentrations is presented.

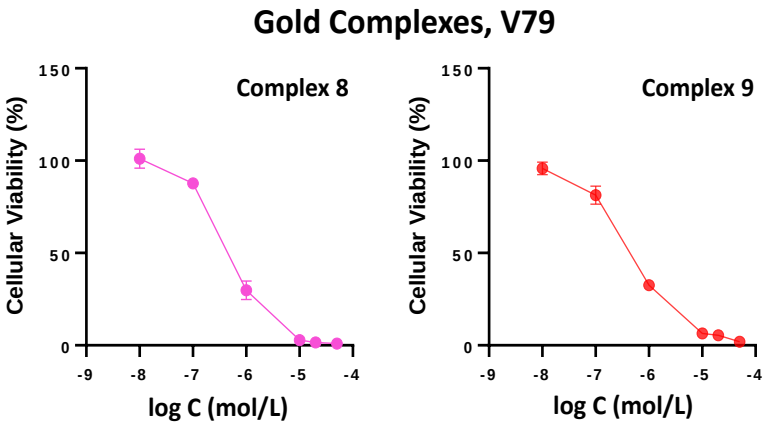

Figure C.11: Dose-response curve obtained with GraphPad Prism software (vs. 5.0) for V79 cells treated with the copper complexes 8 and 9. The cellular viability *vs.* treatment concentrations is presented.

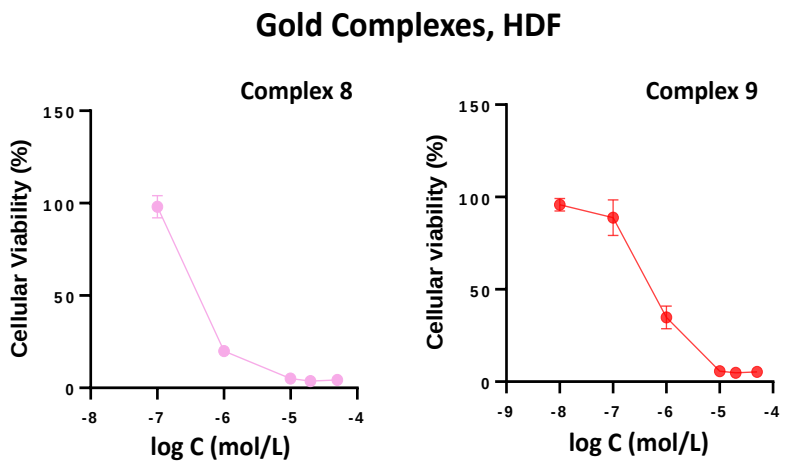

Figure C.12: Dose-response curve obtained with GraphPad Prism software (vs. 5.0) for HDF cells treated with the copper complexes 8 and 9. The cellular viability *vs.* treatment concentrations is presented.

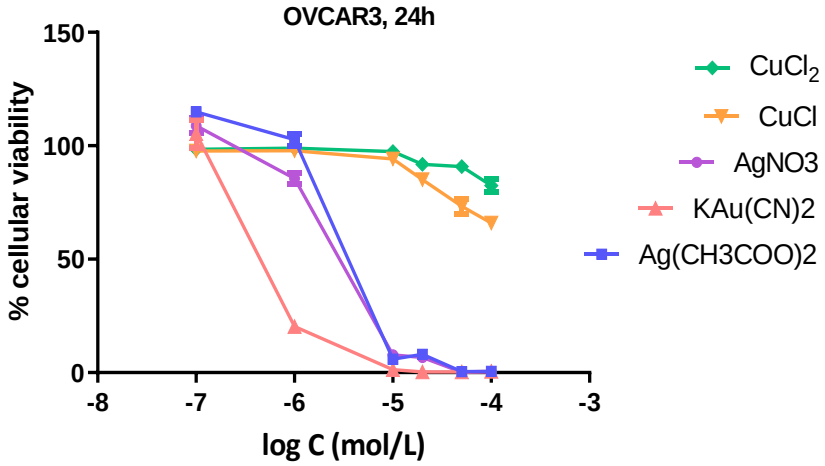

Figure C.13: Dose-response curve obtained with GraphPad Prism software (vs. 5.0) for OVCAR3 cells treated with the metal precursors. The cellular viability *vs.* treatment concentrations is presented.